AMINO ACID CONJUGATED ALGINATE-GRAPHENE OXIDE SCAFFOLDS

by

Ecem Şahin

B.S., Biomedical Engineering, Yeditepe University, 2013

Submitted to the Institute of Biomedical Engineering
in partial fulfillment of the requirements
for the degree of
Master of Science
in
Biomedical Engineering

Boğaziçi University
2017

ACKNOWLEDGEMENTS

I would like to express my gratitude and thanks to my thesis advisor Assoc. Prof. Dr. Bora Garipcan for his continued interest and support in the present work. This thesis would not have been possible without his guidance and support.

I would also like to thank my co-advisor Assist. Prof. Dr. Ayşe Ak for her guidance and support.

I would like to thank my committee members Assist. Prof. Dr. Esin Öztürk Işık, Assist. Prof. Dr. Duygu Ege and Assist. Prof. Dr. Sedat Odabaş for their contribution and constructive comments.

I would like to thank also Anton Paar Laboratory Instruments for their contribution in the rheometry characterization of this thesis.

Special thanks to my dear friends Fatoş Nacar and Elif Dönmez, for helping me and giving me morale support when I needed. And I would like to thank the group members of Bio^3 Research LaBORAtory for their smiling faces and help when working on my thesis project in the laboratory.

Last but not least, I would like to thank my family for their endless love and support through all my life.

ACADEMIC ETHICS AND INTEGRITY STATEMENT

I, Ecem Şahin, hereby certify that I am aware of the Academic Ethics and Integrity Policy issued by the Council of Higher Education (YÖK) and I fully acknowledge all the consequences due to its violation by plagiarism or any other way.

Name :

Signature:

Date:

ABSTRACT

AMINO ACID CONJUGATED ALGINATE-GRAPHENE OXIDE SCAFFOLDS

In this thesis, fabrication and characterization of neat alginate and alginate/graphene oxide (GO) composite 3D porous scaffolds were investigated in order to achieve a material suitable for wound care applications with enhanced properties such as biocompatibility, high mechanical strength, stability, high absorbance and positive cell behaviour. Alginate (Al) was used as the main polymer and GO was used as additive. L-Cysteine (Cys) was conjugated on GO in order to enhance biocompatibility. Initially, neat Al scaffolds were fabricated by ionic crosslinking ($CaCl_2$ as cross-linker) and lyophilisation. Then GO (1mg/ml) was added to the structure and Al/GO scaffolds with different crosslinker concentrations (0.01-0.03 M) were fabricated in order to determine optimal crosslinker concentration. Next, 0.03M crosslinker concentration was kept constant and scaffolds with different GO concentrations (0.5-2 mg/ml) were prepared in order to determine optimal GO concentration. Finally, Cys was immobilized to GO (1:1 ratio) and Al-3/CysGO-0.5 scaffold was fabricated. FTIR and SEM were used for the characterization of Al/GO scaffolds. Swelling ratio and porosity were investigated by conducting swelling test. Viscoelasticity of the non-lyophilized hydrogels was investigated with rheometry method. Viability of fibroblast cells was investigated by MTT assay. According to the results, adding GO to the structure provided stability and immobilization of Cys increased biocompatibility, and a porous, more stable material with high absorbance, biocompatibility and positive cell response was obtained.

Keywords: Alginate, 3D scaffold, graphene oxide, wound healing, composite.

ÖZET

AMİNO ASİT İMMOBİLİZE ALJİNAT/GRAFEN OKSİT DOKU İSKELESİ

Bu tezde, yara tedavisinde kullanılabilinecek biyouyumluluk, yüksek mekanik kuvvet, kararlılık, yüksek emicilik ve pozitif hücre tepkisi özellikleri gelişmiş düz aljinat ve aljinat/grafen oksit (GO) kompozit 3B gözenekli yapıda doku iskeleleri üretilmiş ve karakterizasyonu yapılmıştır. Aljinat (Al) ana polimer olarak kullanılırken, GO mekanik kuvveti ve kararlılığı arttırıcı yardımcı malzeme olarak kullanılmıştır. Biyouyumluluğu arttırmak amacıyla L-Sistein GO yapısına immobilize edilmiştir. İlk önce, iyonik çapraz bağlama ($CaCl_2$ çapraz bağlayıcı) ve liyofilizasyon yöntemiyle düz Al doku iskeleleri üretilmiştir. Sonrasında yapıya sabit oranda (1mg/ml) GO eklenip farklı çapraz bağlayıcı konsantrasyonları (0.01-0.03 M) kullanılarak kompozit Al/GO doku iskeleleri üretilmek suretiyle optimum çapraz bağlayıcı konsantrasyonu belirlenmiştir. 0.03M seçilerek devam edilmiş ve farklı GO konsantrasyonlarında (0.5-2 mg/ml) doku iskeleleri üretilerek optimum GO konsantrasyonu belirlenmiştir.0.5 mg/ml seçilerek devam edilmiş ve GO yapısına L-Sistein (1:1 oranında) immobilize edilerek Al-3/CysGO-0.5 doku iskeleleri üretilmiş ve biyouyumluluk artışı amaçlanmıştır. Al/GO doku iskelelerinin karakterizasyonu için FTIR ve SEM yöntemleri kullanılmış, liyofilizasyon öncesi hidrojellerin viskoelastik özellikleri reometre yardımı ile analiz edilmiştir. Fibroblast hücrelerinin canlılığı MTT analiz yöntemi ile ölçülmüştür. Sonuçlara gore, gözenekli yapıda, yüksek emicilikte, daha stabil ve biyouyumlu bir malzeme elde edilmiştir. Yapıya GO eklenmesi mekanik kuvveti ve kararlılığı, L-Sistein ise biyouyumluluğu arttırmıştır.

Anahtar Sözcükler: Aljinat, 3B doku iskelesi, grafen oksit, yara iyileşmesi, kompozit.

TABLE OF CONTENTS

LIST OF FIGURES

LIST OF TABLES

LIST OF SYMBOLS

G’	Storage Modulus
G”	Loss Modulus
Tanδ	Loss Factor
DI	Deionized
C	Carbon
H	Hydrogen
O	Oxygen
Ca	Calcium
Ba	Barium
Mg	Magnesium
Fe	Iron
Sr	Strontium
W	Weight
V	Volume
ρ	Density

LIST OF ABBREVIATIONS

ECM	Extracellular Matrix
CNT	Carbon Nanotubes
TIMP	Tissue Inhibitors of Metalloproteinases
IUPAC	The International Union of Pure and Applied Chemistry
M Block	Mannuronic Acid Block
G Block	Guluronic Acid Block
GO	Graphene Oxide
Al	Alginate
CysL	Cysteine
GSH	Glutathione
hMSC	Human Mesenchymal Stem Cell
PAM	Polyacrylamide
3D	Three dimensional
FTIR	Fourier Transform Infrared Spectroscopy
SEM	Scanning Electron Microscopy
MTT	3-(4,5-Dimethylthiazol-2-Yl)-2,5-Diphenyltetrazolium Bromide
FBS	Fetal Bovine Serum
DMEM	Dulbecco's Modified Eagle Medium
PBS	Phosphate-buffered Saline
DI	Deionized Water
TCP	Tissue Culture Plate

1. INTRODUCTION

1.1 Motivation

Wound care and healing remain to be common and critical topics due to the aspects such as increasing rate of type II diabetes and obesity, and aging populations with low birth rates. Hence emerges the necessity of more efficient and low cost wound care approaches [1].

Due to several challenges that physicians face including immunologic problems in the host and the undesirable microorganisms in the wound site such as bacteria, wound care becomes a global concern [2]. These kinds of pathophysiologic and metabolic settings can change the normal progression of the wound healing process, causing delayed or impaired healing and resulting in non-healing, chronic wounds [3]. In particular, the bacteria have presented a serious challenge in the hospital environment for many years. These organisms cause severe and hostile infections in the wound site [2].

Considering the importance of the topic and the need of an efficient wound care material that corresponds to the required properties such as non-toxicity, biocompatibility and antimicrobial activity, several approaches have been studied.

Three-dimensional porous polymeric scaffolds are widely preferred in biomaterials studies as they provide sufficient space and surface for cell adhesion and growth. Wound healing is a prominent application for these kinds of scaffolds [4]. An ideal artificial scaffold should: reduce into non-toxic substances which can be removed from the wound site, be able to keep a moist healing environment whilst eliminating excess exudate, permit oxygen permeation, have easy application and removal, low cost, and also should have adequate porosity and pore size that cells can adhere, migrate and proliferate [5].

Collagen is a natural polymer that is utilized in wound care applications. Burke et al., 1982 reported in their study with a bilayer of cross-linked collagen type I and chondroitin 6-sulfate isolated from shark skin that the matrix attracts dermal fibroblasts, which produce new extracellular matrix (ECM) to the wound site and facilitate healing [6].

Chitosan is another natural polymer utilized in wound healing applications due to its ability to regulate wound environment [7, 8]. Chou et al. (2003) and Okamotoa et al. (2003) reported in their studies that chitosan stimulates adhesion, mobilization and aggregation of platelets and erythrocytes towards wound site to accelerate clotting [9, 10].

Alginate is a polysaccharide obtained from brown algae and some bacteria, which has several applications as a natural biomaterial [11]. It is utilized in biomedical field due to its advantageous properties, including facility of gelation and biocompatibility. Alginate hydrogels are widely studied in wound healing under the moist healing approach, also in drug delivery, and tissue engineering to date, thanks to their similar structure to the tissue extracellular matrix (ECM) [12, 13].

There are several alginate-based wound dressings commonly used for use in dealing with a variation of high exudate wound types, such as chronic wounds [14].

Sweeney et al. (2012) reported that alginate dressings diminish microbial bioburden and draw back proteinases [15]. Alginate as a natural polymer is utilized in wound management due to its properties such as creating a moist environment for the wound, high absorbency, and functioning as a hemostat. Pirone et al. (1992) reported that if enough calcium ions in the gluronic and mannuronic acid groups are exchanged with the sodium ions in the blood or exudate in the wound site, the alginate forms a gel that provides a moist environment for the wound by swelling and partly dissolving [16].

Furthermore sufficient mechanical strength is a key factor in such applications to preserve integrity for cell survival. Since pure alginate scaffolds have some deficiencies such as uncontrollable degradation, lack of cell interactions, and low mechanical strength, carbon materials such as graphene oxide (GO) and carbon nanotubes (CNT) are used to compensate these features by producing composite structures [17].

GO is a non-toxic, biocompatible and hydrophilic material compared to CNT, and has no cytotoxic effect (when used in moderate amounts) with cells such as human lung carcinoma epithelial cells, mice and human fibroblasts as indicated by researches to date [18, 19]. As a member of the carbon nanomaterial family, graphene oxide has the chemical and physical properties so that biomolecules such as amino acids, nucleic acids, peptides and aromatic chemical compounds can bind [20].

L-Cysteine is a semi-essential protein with a thiol group. It is produced from methionine and serine in blood [21]. It is metabolically significant with is functions such as detoxification, anti-aging and anti-oxidation [22]. It also plays significant role as cofactor in collagen synthesis and it has indicated to have a positive effect on wound healing process in rats with protein deficiency [23].

1.2 Objectives

In this thesis, alginate-graphene oxide 3-D scaffolds were produced to evaluate the application in wound healing treatment. In order to enhance the mechanical property of Ca^{2+} cross-linked sodium alginate scaffolds, graphene oxide (GO) was added to the structure. Also, L-Cysteine amino acid was added to improve the biocompatibility of the scaffolds. Cellular behaviour such as proliferation and viability were examined. The main objectives of this thesis are:

- To prepare and characterize Al, Al/GO and Al/CysGO, scaffolds.
- To enhance the mechanical property and biocompatibility by adding GO and then L-Cys amino acid to the alginate structure.
- To investigate L929 fibroblast cell behavior on prepared scaffolds by using MTT Assay.
- To advance the use of sodium alginate based scaffolds as a wound healing material.

1.3 Outline

The thesis is presented as follows: In chapter 2, background information about the concept of wound healing, general properties and biomedical applications of alginate, general overview of GO, and general information about the amino acid are given. In chapter 3, the experimental procedures are explained. In chapter 4, the results are presented. In chapter 5, the discussion of the results is given.

2. BACKGROUND

2.1 Wound Healing

2.1.1 Types of Wounds

A wound is a disturbance in the epithelial integrity of skin tissue, which in some cases, comes with disturbance of the function and structure of tissue underneath [24]. Wounds can be caused by thermal or physical damage as well as an existing medical or physiological condition [1].

Wounds are classified into two groups: open (excisional) wounds and closed (incisional) wounds.

- Lacerations, surgical wounds, cutting-pricking tool wounds, insect stings and bites, gunshot wounds, radionecrosis, vascular neurological and metabolic wounds are classified as open wounds. Excluding lacerations, severe damage to the underlying tissue is observed. But in laceration wounds, skin and hypodermic tissue have been gravely damaged, while deep tissue is healthy [25].
- Abrasion, hematoma and contusion are classified as closed wounds. Harm to small blood vessels, soft tissue and deep tissue are observed in contusion type wounds [26].

Wounds can also be classified considering the nature of the repair process: acute wounds and chronic wounds. While acute wounds usually heals fully within the estimated time interval (8-12 weeks) with least scarring, chronic wounds heal slowly or fail to heal because of an underlying medical condition such as diabetes, infections, malignancies etc., frequent insults to the wound or patient related reasons [1].

2.1.2 Phases of Natural Wound Healing

The wound healing process is traditionally divided into four overlapping phases: hemostasis (or haemostasis), inflammation, proliferation, remodeling and later on scar maturation (Figure 2.1).

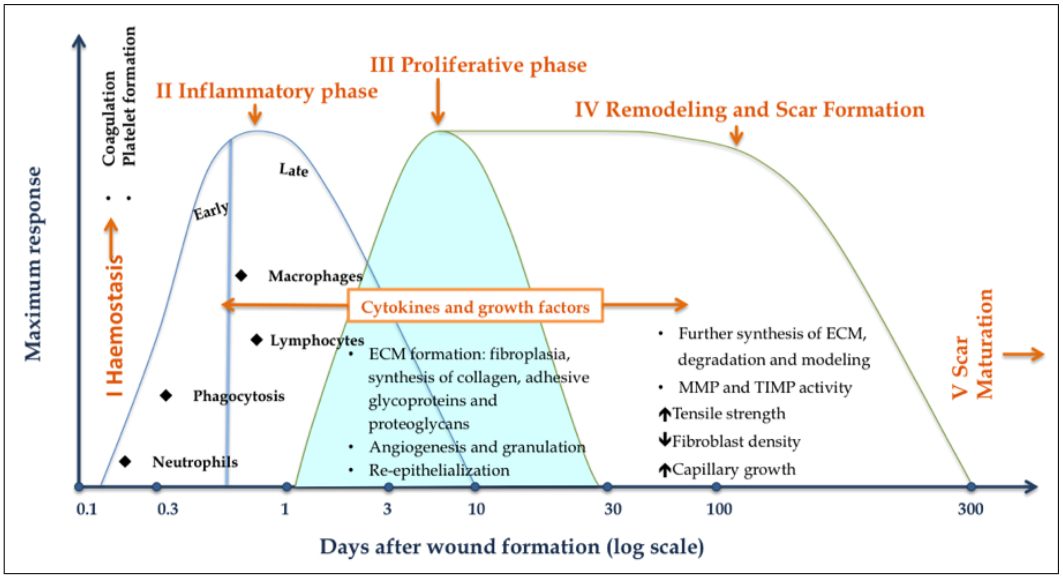

Figure 2.1 Phases of wound healing. ECM: Extracellular matrix; MMP: Metalloproteinases; TIMP: Tissue inhibitors of metalloproteinases [24, 27].

The healing process is triggered by the injury immediately and starts with hemostasis.

I Hemostasis comprises a chain of activities that work together to control the bleeding from a wound. Exposure of the blood vessels to the injury triggers the coagulation cascade and vasoconstriction. Consequential clot formation and platelet accumulation prevents additional blood loss [28].

II In the inflammatory phase cytokines activate the macrophages and chemotaxis of monocytes, and incite proliferation of neutrophils and neovascularization. The function of the neutrophils is to protect the wound against infection by phagocytizing bacteria, dead tissue and the existent foreign substances. Macrophages

function as phagocytic cells and also as the primary source of growth factors. Various leukocytes oppose pathogens and create healthy tissue while degrading injured tissue [28].

III In the proliferation phase fibroblasts are attracted to the wound location by the macrophages and neutrophils. They enable the formation and remodeling of the extracellular matrix. Hyaluronic acid assists the cell migration and makes the tissue resistant to deformation by absorbing water [28].

IV In the remodeling phase type III collagen is substituted with type I collagen, which leads to fibrosis or scars [28]. Both collagen synthesis and lysis happen at a greater rate compared to non-wounded tissue [29]. TIMPs and metalloproteinases enable the remodeling of ECM. This phase continues for months.

Alterations in either of the inflammatory, proliferative or remodeling phase could result in chronic wounds. And abnormalities in proliferative or remodeling phase result in hypertrophic scars and keloids [24].

2.2 Wound Treatment and Materials Used For Wound Healing

Wound care and wound healing technologies is an ever-growing field with the improvement of biomedicine, materials science, and tissue engineering [30].

There are numerous wound dressing materials used to treat both internal and external wounds such as gauzes, synthetic dressings, topical medicinal formulations as well as hydrogels, hydrocolloids and foams etc. [28]. Traditionally wound dressings primarily served just to stop the bleeding, provide a dry environment via evaporation of wound exudates and protect the wound from bacteria and infections [31]. Gauzes, lint, natural and synthetic bandages and cotton wools were used as wound care instruments [1]. For example, gauze has several disadvantages including damaging newly made epithelium with removal and resulting in swift dehydration of the wound bed [32, 33]

and leakage of wound exudate causing infections [25]. The reason for their popularity is their low cost and availability.

However, modern dressings head towards materials that can maintain a moist and airy environment since it is generally accepted that a warm, and moist environment incites quick healing and current products are designed to satisfy these requirements unlike the traditional dressings, which have no effect on the healing process [34, 35].

2.2.1 Functional Characteristics Of An Ideal Wound Dressing

In the past traditional wound dressings such as gauzes, lint and cotton bandages were used, the only purpose being covering and protecting the wound from external factors and stopping the excessive bleeding. However search for suitable materials to facilitate and accelerate the wound healing process and to prevent keloid and scar formation came into prominence, because of the drawbacks of traditional materials and tissue transplants (xenograft, allograft and autograft) such as risk of infection and stability problems [25].

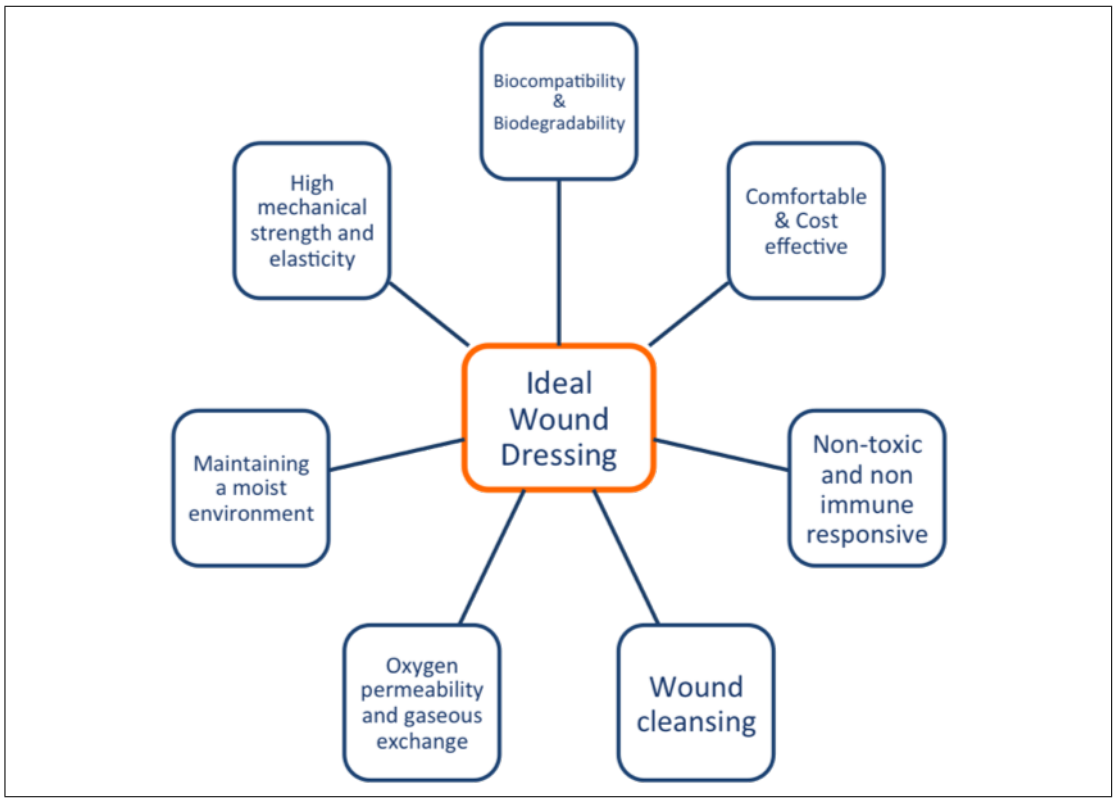

Figure 2.2 Characteristics required in an ideal wound dressing to optimize the wound healing process [31, 36].

Required properties of an ideal wound dressing is shown in Figure 2.2. Since in practice, there is no perfect biomaterial, choosing the proper dressing material matching the needs of a specific wound is important [37].

There are three groups of wound dressing products according to their type of action: passive products (traditional products like tulle and gauze), interactive products (generally transparent polymeric forms and films that provide water vapor and oxygen permeation also preventing bacterial infection, usually used for low exudate wounds) and bioactive products composed of materials such as alginate, chitosan, collagen, proteoglycan, and silk protein [36].

2.2.2 Polymers Used In Wound Care Applications

Biopolymers are macromolecules formed by living organisms as defined by IUPAC [38]. They are biodegradable polymers.

Polymers can be divided into two groups: synthetic polymers and natural polymers. Natural polymers are polysaccharides (chitosan, chitin, alginate, cellulose) and proteins (albumin, collagen, silk sericin, silk fibroin) [39].

Thanks to their properties like good biodegradability, biocompatibility and hydrophilicity natural polymers are suitable for new tissue formation eliminating inflammation [39]. Also being less expensive and safer compared to synthetic materials makes natural polymers eligible for researchers in tissue engineering field [40].

There are numerous dressing forms being studied on currently. Using biodegradable and biocompatible polymers, microspheres, nanofibrous matrices, hydrogels, and foams are being developed. Polymeric scaffolds with molecular and cellular modulators to motivate wound healing are also available for tissue engineering applications [41]. Having an open porous structure and good mechanical strength, they offer an ideal microenvironment for cell migration, differentiation and proliferation [42].

Various synthetic and natural polymers are utilized in the design of artificial dressing materials. Among the most commonly used of these are given in Table 2.1 and Table 2.2.

Table 2.1
Synthetic polymers and wound healing applications.

SYNTHETIC POYLMERS	ADVANTAGE/APPLICATION
Polyurethane and its derivatives	Copolymers with urethane groups. A kind of non-toxic polyurethane which is known to quicken repithelization was utilized for treatment of wound and burns by Wright et al. [43, 44].
Teflon	A non-carcinogenic inert polymer synthesized via polymerization of tetrafluoroethylene at high pressure and temperature. It is easily applicable to the damaged tissue since it is easily shapeable once applied low pressure [25].
Silicone	A low allergenic material that has low,toxicity, high biocompatibility, which makes it a demanding alternative in,biomedical applications. One of the many uses of silicone in biomedical,applications is in the design of implant elastomers in soft tissue repair. It,is also utilized as wound support material in critical burns and wounds,because of its high compatibility with tissues [25, 45].

Table 2.2
Natural polymers and wound healing applications.

NATURAL POYLMERS	ADVANTAGE/APPLICATION
Collagen	Most abundant protein found in the extracellular matrix and offers mechanical stability, strength, and elasticity to organisms. Excellent biocompatibility, biodegradability and low antigenicity compared to other natural polymers. Takes part in the wound healing by stimulating the molecular and cellular cascades, and contributing to new tissue formation and wound debriment. Applications in biomedical sciences including sutures and catguts, sponges for the hemostasis and coating of joints, wound dressing materials and suspensions for dermal injection [41, 46, 47]
Chitosan	A poly-N-acetyl-glucosaminoglycan formed by alkaline deacetylation of chitin. A biocompatible material that shows low thrombogenicity and low toxicity. It is believed to accelerate granulation in the proliferative phase and also fibroblast formation having a haemostatic effect. Used in wound healing applications in the form of fibres, hydrogels, powders, films and micro/nanoparticles [40, 48, 49].
Fibroin (Silk Protein)	A natural polymer obtained from silk fibre. It exhibits good oxygen and water vapor permeability, biodegradability, flexibility, exudate absorption, easy modification thanks to functional groups and minimal inflammatory response. Used in form of matrices, fibres, gels, powders, films, and scaffolds in biomedical applications [40].
Alginate	A naturally derived linear polysaccharide copolymer, which contains the monomers (1-4)-linked β -D-mannuronic acid (M units) and α -L-guluronic acid (G units). Can be used in forms of soft, elastic gels, scaffolds, foams, multilayers, fibres and nanoparticles. It is non-toxic and biocompatible. It provides a moist environment to the wound and minimizes bacterial infection and has properties such as hemostatic capability and facility of gelation. Alginate promotes tissue formation and repithelization. Its swelling property makes it preferable for exuding wounds [50–53]

2.3 Alginate Overview

Alginate is a naturally derived linear polysaccharide copolymer, which contains the monomers (1-4)-linked β -D-mannuronic acid (M units) and α -L-guluronic acid (G units) [53]. These blocks are typically assembled in three different forms: repeated G blocks (-G-G-), repeated M blocks (-M-M-) or alternating blocks (-M-G-M-G) as illustrated in Figure 2.3. Since alginates are extracted from a number of sources, M and G content and the length of each block differ from batch to batch [54]. Several properties of alginate and its derivatives such as swelling, viscoelasticity and transmittance, are notably affected by the M/G units ratio [55].

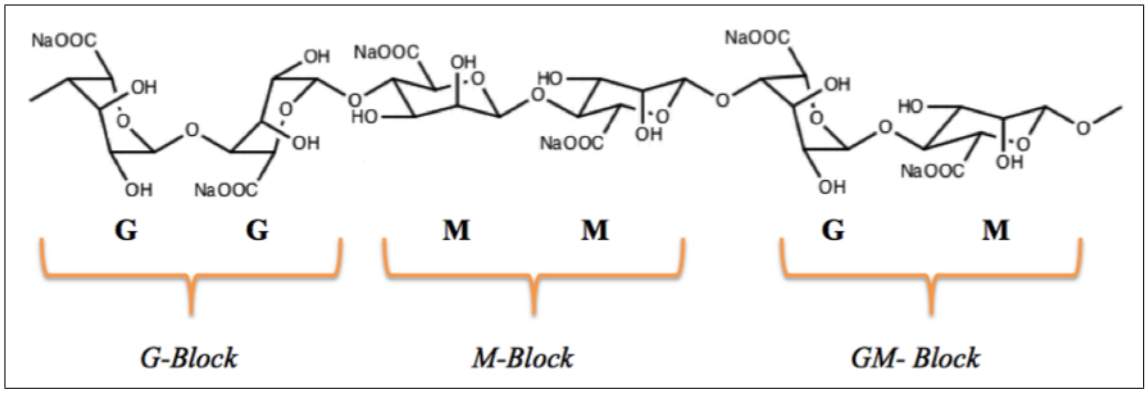

Figure 2.3 Schematic diagram of sodium salt of alginate composed of (1-4)-linked β -D-mannuronic acid (M block) and α -L-guluronic acid (G block), and alternating blocks.

When monovalent ions (i.e. sodium) are attached to the carboxylic groups ionically, alginate salt (e.g. sodium alginate), is formed as shown in Figure 2.3.

When divalent cations, such as Ca^{2+}, Mg^{2+}, Fe^{2+}, Ba^{2+}, Sr^{2+} are present ionic inter-chain bridges are formed, thus reversable alginate gels are formed in aqueous media [51]. The gelation and crosslinking of the polymers are mostly accomplished via the exchange of ions from the guluronic acids with the divalent cations (most commonly Ca^{2+}). The stacking of these guluronic groups forms the specific egg-box structure illustrated in Figure 2.4. Since the carboxylic groups of the G blocks go under crosslinking with cations, alginates rich in G residues produce more rigid gels.

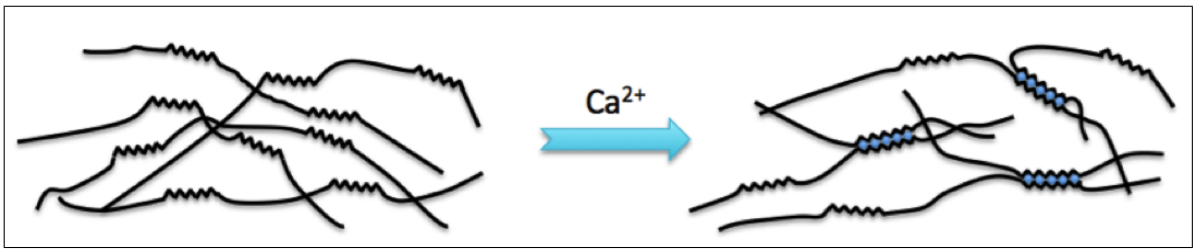

Figure 2.4 Schematic diagram of the egg-box structure in the presence of Ca^{2+}.

There are multiple sources of seaweeds as well as some bacteria from which the alginates can be extracted such as: Laminaria sp., Macrocystis sp., Lessonia sp., Ascophyllum etc. [27]. Alginate is obtained by treating seaweed with aqueous alkali solutions (usually NaOH), filtering and subsequently adding calcium chloride or sodium chloride. The resulting salt, when treated with diluted HCl, yields alginic acid [56].

2.4 Applications of Alginate

Alginates have various application areas such as food, textile printing, paper, pharmaceuticals and welding rods [27]. As biomaterials, alginates can be used in forms of soft, elastic gels, scaffolds, foams, multilayers, fibers and nanoparticles at in situ conditions so that cell function and viability are provided. Ultrapure alginates are available which eliminate the immunogenicity and toxicity of industrial grade alginates. Also bioactive and inert alginates are available with no adverse effects. Its versatility and biocompatibility draws attention for biomedical applications [52].

However, alginate shows some deficiencies such as poor mechanical strength and loss of structural integrity that may limit its application as a biomaterial [57]. There are ongoing researches to improve its performance and overcome these deficiencies. Researches show that mixing alginates with polymers such as chitosan [58], pectin [59] or polyvinyl alcohol resulted in minor effect [60].

Carbon nanomaterials are also evaluated as an alternative to compound with alginate. Carbon nanotubes (CNT), reported by Kawaguchi et. al., are shown to advance the mechanical properties of alginate, as Al/CNT hydrogels were mechanically stronger than Al hydrogels [61]. Yet, CNT show poor solubility and toxicity which are undesired for biomedical applications [62, 63].

At this point graphene oxide (GO) comes forward as an alternative to consider with its nontoxic, hydrophilic and biocompatible nature and its structure abundant of oxygen functional groups (i.e. carboxyl, epoxide and hydroxyl groups), which facilitates interfacial interactions [64].

2.5 Alginate in Wound Care

Alginate has been utilized as a wound dressing material for more than 30 years, but its history dates back to ancient Rome, where seaweed was used to treat wounds [65]. There are multiple sources of seaweeds as well as some bacteria from which the alginates can be extracted such as: Laminaria sp., Macrocystis sp., Lessonia sp., Ascophyllum etc. [27].

The main reason of using alginate in wounds is its ability to absorb fluid 15-20 times of its own weight [66]. Hence, alginate outshines other alternatives for heavily and normally exuding wounds by managing the wound exudate and maintaining a moist environment for healing process. However it is not convenient to use with dry wounds or wound with minimal exudate, surgical implantations, and third degree burns since it may cause the wound to dry out [12, 40].

Furthermore, alginates are able to decrease wound pain, and the bioburden of the wound, absorb proteinases and reduce odor [67, 68].

2.6 General Overview of Graphene

Graphene is a two-dimensional, one atom thick (0.35 to 1.6 nm in thickness) planar sheet composed of sp^2 bonded carbon atoms, packed compactly in honeycomb crystal lattice form [69]. The IUPAC gives the definition of graphene as a single carbon layer of the graphite structure.Its nature is described by analogy to a polycyclic aromatic hydrocarbon of quasi-infinite size [70].

As a carbon nanomaterial (CNT) with favorable unique properties such as strong mechanical strength (about 1100 GPa), facility of functionalization, outstanding biocompatibility, high electrical conductivity (1738 siemens/m), high surface area (2630 m^2/g), and thermal conductivity (5000 W/m/K) has drawn increasing attention over the last decade [71].

In addition it has high intrinsic mobility (200 000 cm^2 v^{-1} s^{-1}) and high Young's modulus (1.0 TPa) [72]. A single layer non-defected graphene, has fracture strength and Poisson's ratio 130GPa and 0.149 GPa correspondingly. Thanks to its excellent mechanical strength, graphene is utilized to strengthen polymeric scaffolds [73, 74].

The ability to adsorb various aromatic biomolecules via π - π stacking interaction and/or electrostatic interaction, makes graphene preferable for applications such as biosensors and loading drugs [71].

2.7 Graphene Oxide

Graphene oxide (GO) is the highly oxidized form of graphene containing large number of functional groups such as carboxyl group (-COOH) in the edges and hydroxyl (-OH) and epoxy (-O-) group in the basal planes (Figure 2.5), that makes GO relatively hydrophilic, easy to disperse in water and other solvents, and easy to modify [75].

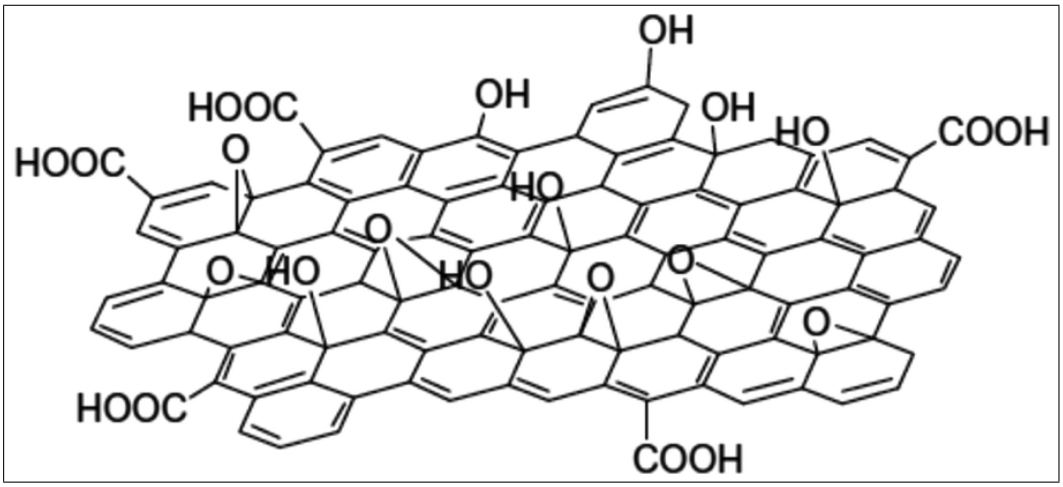

Figure 2.5 Schematic representation of graphene oxide structure [76].

GO can be synthesized from graphite flakes using the Brodie , the Staudenmaier or Hummers method. As GO is synthesized from low-cost graphite, it has lower cost compared to other CNTs, and this has stimulated work on GO/synthetic polymer composites [77, 78].

Graphene oxide is a good alternative to other carbon nanomaterials and polymers such as chitosan and pectin when it comes to produce high performance composites that eliminate deficiencies of alginate [64].

2.8 Application of Graphene and Graphene Oxide in Biomaterial Science

In tissue engineering mechanical strength of a scaffold is a key property. Graphene is a favorable nanomaterial to integrate to several scaffolds due to its unique mechanical properties (Young's Modulus of 1000 GPa, Poisson's ratio of 130 GPa and fracture strength of 0.149 GPa) [79]. Excellent electrode property of graphene may come handy to carry electrical currents used for differentiation and neural stimulation [80]. Studies had shown that graphene has the capability to stimulate differentiation of hNSCs to

neurons and oligodendrocytes, hMSCs to adipocytes and also to prompt differentiation in iPSCs towards endodermal line [79].

Graphene and GO also shows antimicrobial activity, which is crucial for wound healing applications. Recent studies had shown that the antibacterial property is caused by synergisticity of membrane disruption and the oxidative stress. In other words, the cell membrane can be agitated by the sharp edges of graphene and lead to leak of cellular substances ultimately resulting in cell death. Liu et. al. also reported that internalization of graphene or GO by bacteria may cause oxidation of GSH that causes oxidative stress [81].

Polymer/graphene nanocomposites express greater electrical, thermal, mechanical, gas barrier, and flame retardant characteristics when compared to the neat polymer. While pristine graphene does not form homogenous composites with organic polymers, GO sheets, being highly rich in oxygen (with carboxyl hydroxyl, epoxide, ketone and diol functional groups on the surface) are more compatible due to ease of functionalization. Moreover the extra carboxyl and carbonyl groups found on the edges of the sheets make GO highly hydrophilic, facilitating it to disperse and water [69].

All these unique properties such as strong mechanical strength, cost efficiency, high surface area, high biocompatibility and ease of functionalization put GO forward for applications such as composites with polymers [71, 77].

So far, Depan et al. reported that composing GO with chitosan (CS), GO/CS nanocomposite scaffolds demonstrate superior mechanical properties, cell growth. Proliferation and attachment when compared to pristine CS scaffolds [82].

Qi et al. reported that GO/poly(vinyl alcohol) nanofibrous scaffolds that they produced possessed enhanced mechanical properties and cell proliferation for osteoblasts compared to pristine poly(vinyl alcohol) [83].

As for Al/GO composites, Wang et al. and Mariana et al. conducted studies producing GO/Al gel beads and GO/Al composite films, respectively, with no interconnected porous construction [60,84]. Al/GO/polyacrylamide (PAM) nanocomposite hydrogel was prepared by Fan et al. Yet it is observed that in natural environment PAM degrades into acrylamide, which is a toxic substance. It is also observed that the pore size of the hydrogel is under 10 μ, making it unsuitable for tissue engineering applications [13].

Thus developing a 3D porous scaffold with good mechanical strength and biocompatibility by utilizing unique properties of GO such as ease of functionalization and combining it with Al shows to be a promising application.

2.9 L-Cysteine

L-cysteine is a semi-essential amino acid, which contains thiol group (Figure 2.6) and plays a significant role in human diet. It is produced from methionine and serine in blood. As a biomarker and an antioxidant, it is broadly used in pharmaceutical and food industry [21]. It has been reported that it has a positive effect on wound healing mechanism [23]. L-cysteine has significant metabolical functions such as detoxification, anti-aging and anti-oxidation. Cysteine also contributes to collagen synthesis as a cofactor. So far trials showed that sulfur containing amino acids such as cysteine and methionine have positive effect on wound healing process in rats with protein deficiency [23].

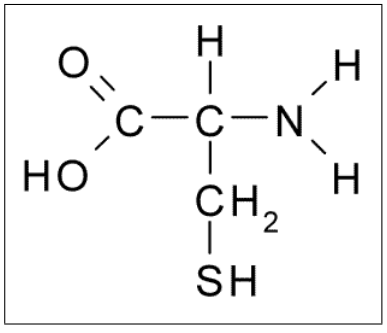

Figure 2.6 Molecular structure of L-Cysteine.

3. MATERIALS AND METHODS

3.1 Fabrication of Alginate (Al) Scaffolds

The Alginate (Al) scaffolds were prepared by using solution mixing and freeze-drying methods as shown in Figure 3.1. 3% w/v (0.12 g) of sodium alginate (Sigma-Aldrich) powder was dissolved in DI water. Calcium Chloride solution (0.03M), (Sigma-Aldrich) was prepared and added to the alginate solution under stirring as a cross linker (4:1 ratio). The solution was mixed in the ultrasonic bath until it is homogenous in order to facilitate and accelerate the gelation process as shown in Figure 3.2. The resulting gel was equally divided into wells of a 24-well plate. The samples were degassed using a desiccator in order to remove the air bubbles in the gels. The plate was cooled at 4 °C overnight. The next day, the plate was kept at −20 °C. for 30 min. Then lyophilized for 7.5 h and Al-3 (alginate with 0.03M of $CaCl_2$) scaffolds were obtained.

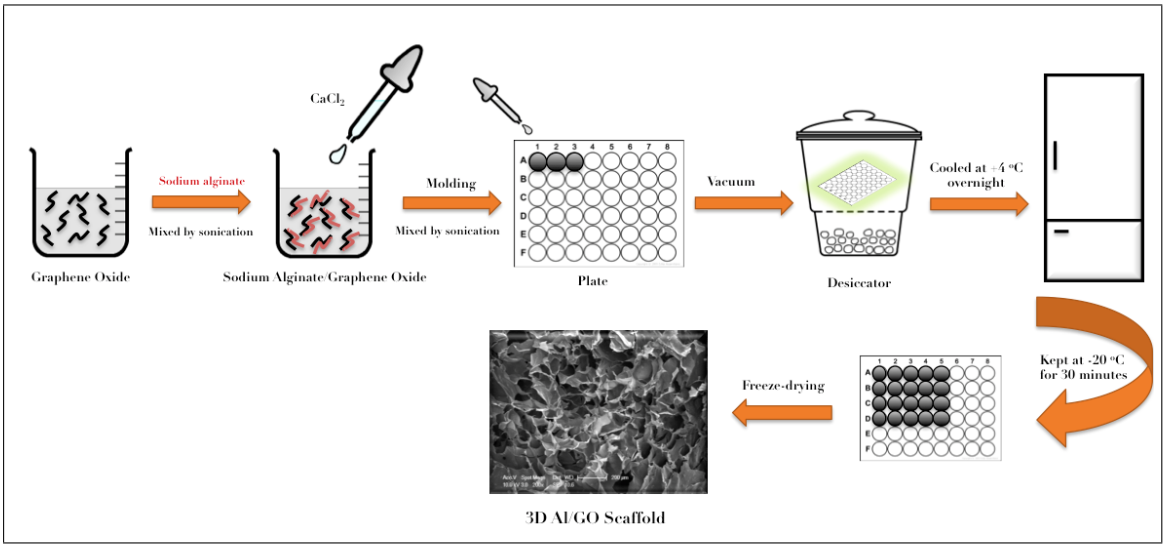

Figure 3.1 Schematic representation of the fabrication process of 3D porous Al/GO scaffolds.

3.2 Fabrication of Al/Graphene Oxide Scaffolds

3.2.1 Optimization of Crosslinker Concentration

The Al/GO scaffolds were prepared by following the same procedure illustrated in Figure 3.1. GO suspension (Sigma Aldrich, 2mg/ml, GO) was used as solvent instead of DI water. It was diluted to 1mg/ml and then sonicated for 15 min. in order to obtain a homogenous suspension. The Al amount was kept constant (0.12 g). Three experimental groups were prepared to determine the optimal $CaCl_2$ concentration. Predetermined concentrations of 0.01 M, 0.02 M and 0.03 M $CaCl_2$ were prepared for three experimental groups and added to the solutions under stirring as cross linker (4:1 ratio). The solution was mixed in the ultrasonic bath until it is homogenous for 20 min. The resulting gel was equally divided into wells of 24-well plate. The samples were degassed by using a desiccator in order to remove the air bubbles in the gels. The plate was cooled at 4 °C overnight. The next day, the plate was kept at −20 °C for 30 min. Then lyophilized for 7.5 h and Al-3/GO-1, Al-2/GO-1, Al-1/GO-1 composite scaffolds with a GO content of 3 wt% was obtained. The integration of GO to the alginate structure is demonstrated in Figure 3.2.

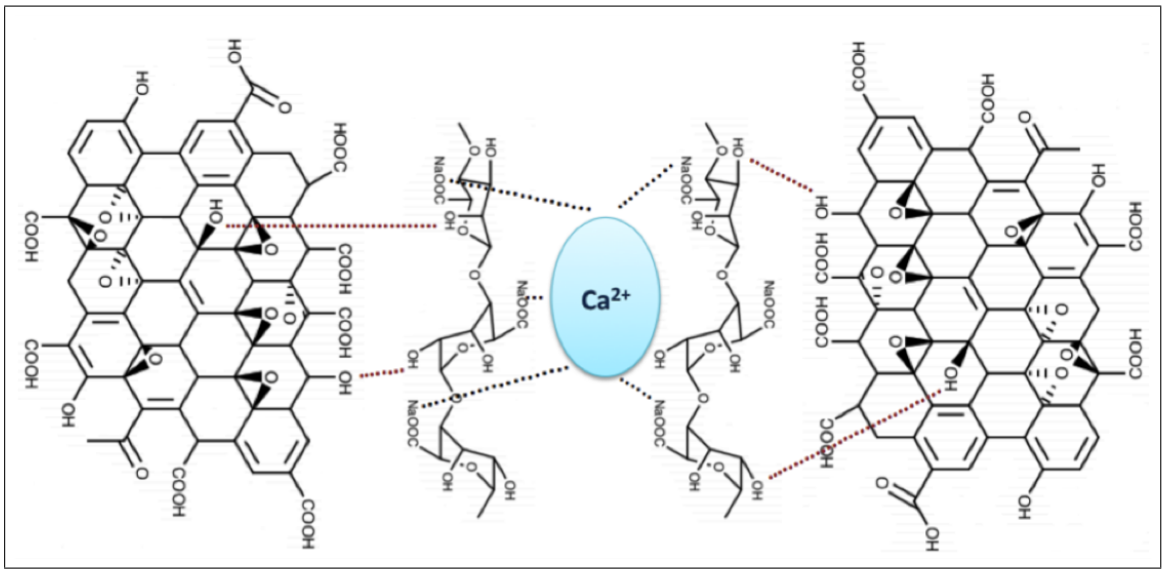

Figure 3.2 Schematic representation of Al/GO composite molecular structure.

3.2.2 Optimization of GO Concentration

The Al/GO scaffolds were prepared following the same procedure with the determined concentration of 0.03 M of $CaCl_2$ as cross linker (4:1 ratio). Three experimental groups were prepared to determine the optimal GO concentration. GO suspension was diluted to the predetermined concentrations of 0.5 mg/ml, 1 mg/ml and 2 mg/ml. The Al amount was kept constant (0.12 g). The solutions were mixed in the ultrasonic bath until homogenous for 20 min. The resulting gels were equally divided into wells of 24-well plate. The samples were degassed by using a desiccator in order to remove air bubbles in the gels. The plate was cooled at 4 °C overnight. The next day the plate was kept at −20 °C for 30 min. Then lyophilized for 7.5 h and Al-3/GO-0.5, Al-3-GO-1 and Al-3-GO-2 composite scaffolds were obtained with a GO content of 1 wt%, 3 wt% and 5 wt% respectively.

3.3 Fabrication of L- Cysteine Conjugated Al/GO Scaffolds

The L-Cysteine conjugated Al/GO scaffolds were prepared following the same procedure illustrated in Fig. 3.1. GO suspension was diluted to determined concentration of 0.5 mg/ml and then sonicated for 15 min. in order to obtain a homogenous suspension. To immobilize L-Cysteine on GO, the carboxylic groups on its surface were activated by adding N-hydroxysulfosuccinimide (0.5 M) and 1-ethyl-3- (3-dimethylaminopropyl)-carbodiimide (0.2 M) to the GO suspension and waiting for 1 h. Then, water-soluble L-Cysteine hydrochloride was added to the solution (1:1 ratio) and incubated at room temperature overnight. Then, CysGO suspension was centrifuged and rinsed thoroughly with DI water to remove excessive L-Cysteine hydrochloride.

The same amount of alginate (0.12 g) was added to the solution. 0.03M $CaCl_2$ was prepared and added to the solution under stirring as cross linker (4:1 ratio). The solution was mixed in the ultrasonic bath until it is homogenous for 20 min. The resulting gel was equally divided into wells of 24-well plate. The samples were degassed by using a desiccator in order to remove air bubbles in the gels. The plate was cooled at

4 °C overnight. The next day the plate was kept at −20 °C for 30 min. then lyophilized for 7.5 h and Al-3/CysGO-0.5 composite scaffolds with a GO content of 1 wt% was obtained.

3.4 Characterization of Al/GO Scaffolds

3.4.1 Fourier Transform Infrared (FTIR) Spectroscopy

Fourier Transform Infrared (FTIR) spectroscopy analysis of sodium alginate powder and lyophilized scaffolds were performed in order to investigate the chemical structure of the scaffolds and the interactions between Al/cross linker, Al/GO and Al/GO/Cys. The measurements were taken within the range of 650-4000 cm^{-1} wavelengths. The FTIR data of the experimental groups Al, Al-1, Al-2, Al-3, Al-1/GO-1, Al-2/GO-1, Al-3/GO-1, Al-3/GO-0.5, Al-3/GO-2 and Al-3/CysGO-0.5 were obtained. The FTIR measurements were perfomed at Hacettepe University Advanced Technologies Application and Research Center using Attenuated Total Reflectance Fourier Transform (ATR- FTIR) spectrophotometer.

3.4.2 Swelling Ratio

Swelling behaviour of the scaffolds was studied conducting the swelling ratio test. The pre-weighted dry scaffolds were each immersed in 4 ml of DMEM cell culture medium in a 6-well plate at room temperature. The plate was covered with lid to minimize loss by evaporation. At pre-designated time intervals of t= 6h, 12h, 24h and 48h the scaffolds were removed and weighed after excessive solution was removed carefully. The swelling ratio was calculated as follows,

$$SR(\%) = \frac{Wt - W_O}{W_O} X100 \tag{3.1}$$

where W_O represents the dry weight of the scaffolds and Wt denotes the measured weight at a specific time point [85, 86].

3.4.3 Porosity

Porosity of the scaffolds was investigated using the liquid replacement method. The pre-weighted dry scaffolds were immersed in DMEM cell culture medium for 12h. Then the scaffolds were weighted after the excessive liquid was removed. The porosity was calculated as follows,

$$\%porosity = \frac{W_t - W_0}{\rho V} X100 \tag{3.2}$$

where W_0 is the initial weight of the scaffold, W_t is the final weight of the scaffold, ρ is the density of the liquid and V is the volume of the scaffold [87].

3.4.4 Characterization of Morphological Properties

The surface and cross section morphology of the porous scaffolds were investigated using Scanning Electron Microscopy (SEM). The surfaces of interest of the samples were covered with a thin layer of gold preceding the imaging. SEM images were obtained at 10.00 kV and 10 mm working distance using diverse magnifications with an interval of 100x - 5000x at Bogazici University Research & Development Center Electron Microscopy and Microanalysis Unit, Istanbul, Turkey.

3.4.5 Characterization of Rheological Properties

The rheological properties of the non-lyophilized hydrogels were investigated in order to observe the effect of cross linker concentration on viscoelasticity. The measurements were taken via Anton Paar MCR Series - MCR 302 Rheometer. Strain controlled - amplitude sweep test method was used with 23 °C test temperature and 10 rad/s angular frequency.

3.5 Cell Culture Studies

In order to investigate effects of prepared scaffolds on cell viability, fibroblast cell line (L929, ATCC, USA) was cultured on tissue culture plate and the cell culture medium that scaffolds were immersed in was interacted with cells. The cell viability of the culture was measured by MTT assay. Approximately 104 cells were cultured onto each well of a 96-well plate. DMEM High Glucose culture medium (Capricorn Scientific) was used after adding 1% v/v antibiotic and 10% v/v Fetal Bovine Serum (FBS).

All samples (for 1^{st} and 4^{th} day) were sterilized prior to cell culture studies. First, both sides of the scaffolds were exposed to UV light for 20 min per side. Then the scaffolds were washed with 0.8 ml of 70% (v/v) ethanol for 20 min and then immersed in 0.8 ml PBS for 30 min. This process was repeated twice [88].

Afterwards the samples in 24-well plate were immersed in DMEM culture medium and placed in the incubator (37 °C, 5% CO_2). L929 cells were cultured in a 96-well plate with the density of 104 cells/well with the sample size 5 for each group including control and placed in the incubator (37 °C, 5% CO_2). After 24 h, cell medium from the samples was transferred onto cells (100 μl /well). Then cell culture plate was placed in the incubator (37 °C, 5% CO_2) again. After 24 h viability of cells was measured by using MTT assay was performed.

The cell viability was also measured at 96 h time point by using a second set of samples. The samples in 24-well plate immersed in DMEM culture medium for 96 h, afterwards, cell medium from the samples was transferred (100 μl/well) onto cells cultured (10^4 cells/well) the previous day. Then cell culture plate was placed in the incubator (37 °C, 5% CO_2) again. After 96 h viability of cells was measured by using MTT assay was performed.

3.6 Statistical Analysis

Statistical analysis was performed by using ANOVA method to define the level of the statistical significance between experimental groups and TCP. The value of $p<0.05$ was considered statistically significant. Tukeys multiple comparison tests was performed. The data were demonstrated to be as means ± standard deviation or standard error.

4. RESULTS

4.1 Chemical Characterization Results

4.1.1 The Fourier Transform Infrared (FTIR) Spectroscopy

FTIR spectroscopy was used to characterize the chemical structure of the prepared scaffolds and the interactions between alginate/$CaCl_2$, alginate/GO and alginate/GO/Cys. The gelation of Al/$CaCl_2$ aqueous solution, integration of GO to the alginate structure and immobilization of L-Cysteine to the GO surface were also investigated.

The results of the FTIR analysis are given from Figure 4.1 to 4.4.

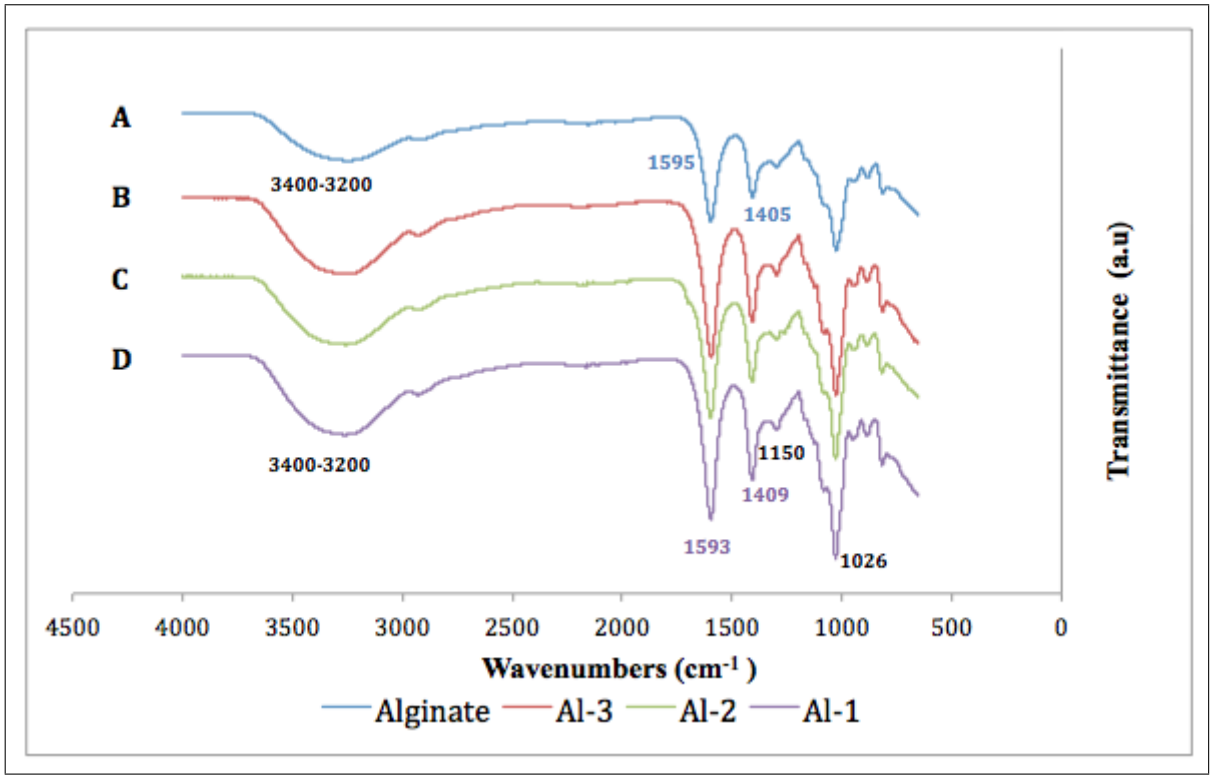

Figure 4.1 FTIR spectra of A) sodium alginate powder, B) Al-3 C) Al-2 and D) Al-1 scaffolds.

FTIR spectra of sodium alginate, and Al/$CaCl_2$ cross-linked scaffolds with $CaCl_2$ molarities of 0.01M, 0.02M and 0.03M were compared (Figure 4.1). In the spectrum of sodium alginate (Figure 4.1, A), stretching vibrations of -OH bonds can be observed in the range of 3200-3400 cm^{-1}. And stretching vibrations of aliphatic C-H can be observed at 2926 cm^{-1}. Dominant absorption bands at 1595 cm^{-1}, and 1405 cm^{-1} correspond to asymmetric and symmetric stretching vibration of carboxylate salt group respectively. The band peak that corresponds to asymmetric stretching vibrations of C-O-C bond which appears at 1150 cm^{-1} shows no change with the introduction of the cross linker $CaCl_2$ .The band peaks observed at 1080 cm^{-1} and 1026 cm^{-1} which indicate the stretching vibrations of the C-O bond of the glycosidic linkage also remained unchanged. (Figure 4.1, B,C,D) The shifts from 1595 cm^{-1} to 1593 cm^{-1} and from 1405 cm^{-1} to 1409 cm^{-1} (Figure 4.1 A,D) were observed.

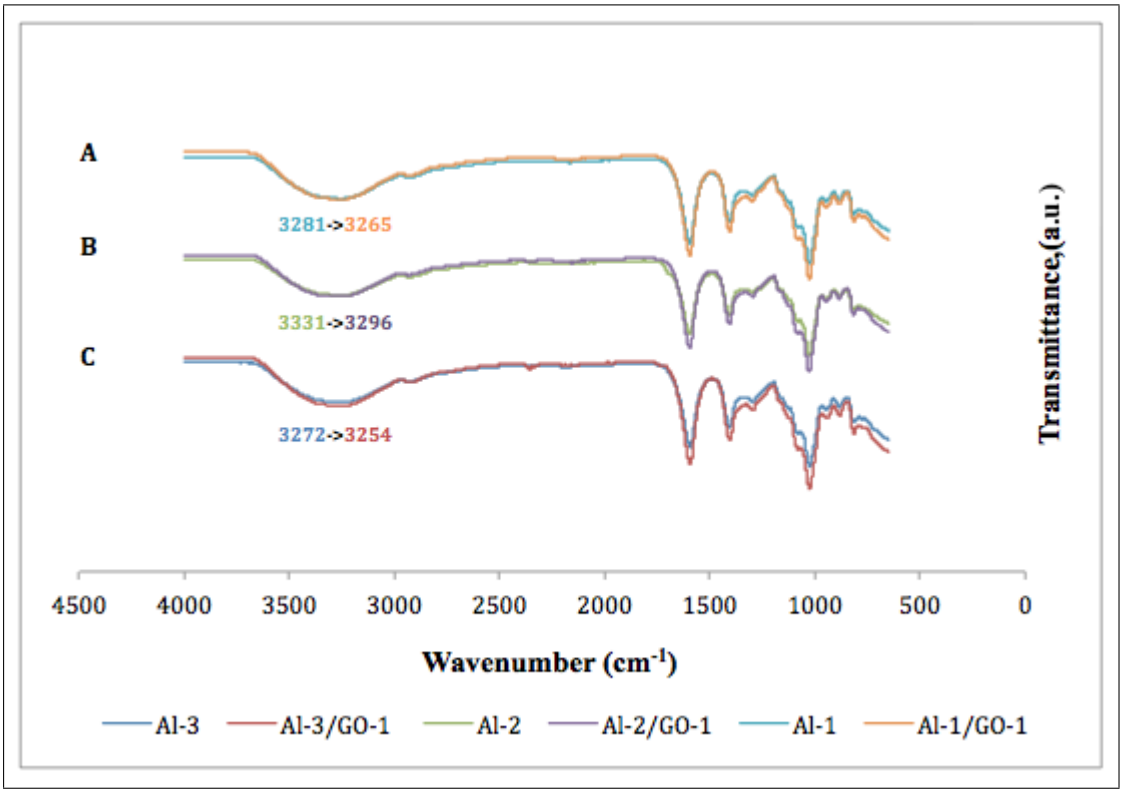

Figure 4.2 FTIR spectra of A) Al-1 and Al-1/GO-1, B) Al-2 and Al-2/GO-1 and C) Al-3 and Al-3/GO-1.

FTIR spectra of Al/GO composites (1mg/ml GO) with different molarities (0.01M, 0.02M, 0.03M) of $CaCl_2$ solution as cross linker were recorded and compared to the spectra of Ca^{2+} cross linked sodium alginate hydrogel with the corresponding molarity of $CaCl_2$ (Figure 4.2). It is observed that the intensity of the band that represents the stretching vibrations of -OH bond has increased additional to Al spectra. Also, -OH absorption bands widened slightly and mildly shifted to lower wavenumbers (0.01M= from 3281 cm^{-1} to 3265 cm^{-1}; 0.02M= from 3331 cm^{-1} to 3296 cm^{-1}; 0.03M= from 3272 cm^{-1} to 3254 cm^{-1}) [17, 60].

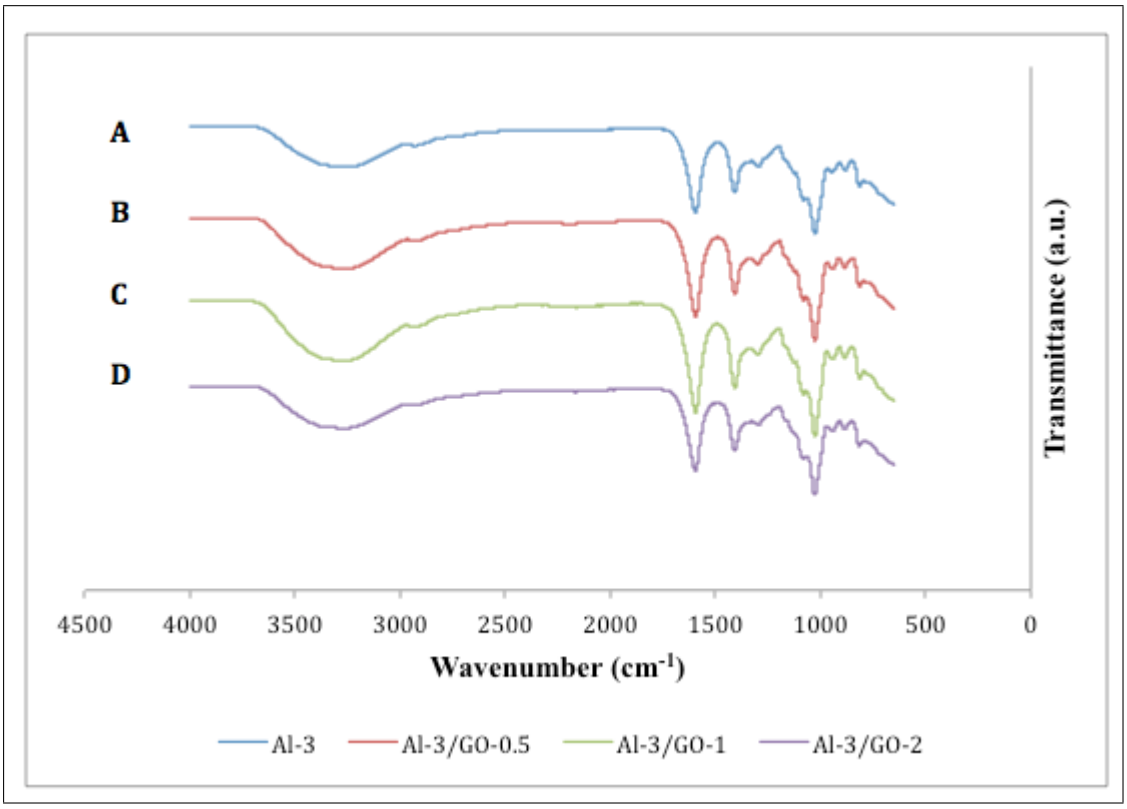

Figure 4.3 FTIR spectra of A) Al-3 B) Al-3/GO-0.5, C) Al-3/GO-1 and D) Al/GO-2 experimental groups.

FTIR spectra of lyophilized scaffolds Al-3, Al-3/GO-0.5, Al-3/GO-1 and Al-3/GO-2 are recorded and compared in Figure 4.3. It was observed that the intensity of then -OH stretching vibration peak increases as the concentration of GO increases.

Also a slight red shift (increase in wavelength) was observed in the same band, which affirms the interfacial adhesion and hydrogen bonding (Figure 3.2) between Al and GO [17, 89].

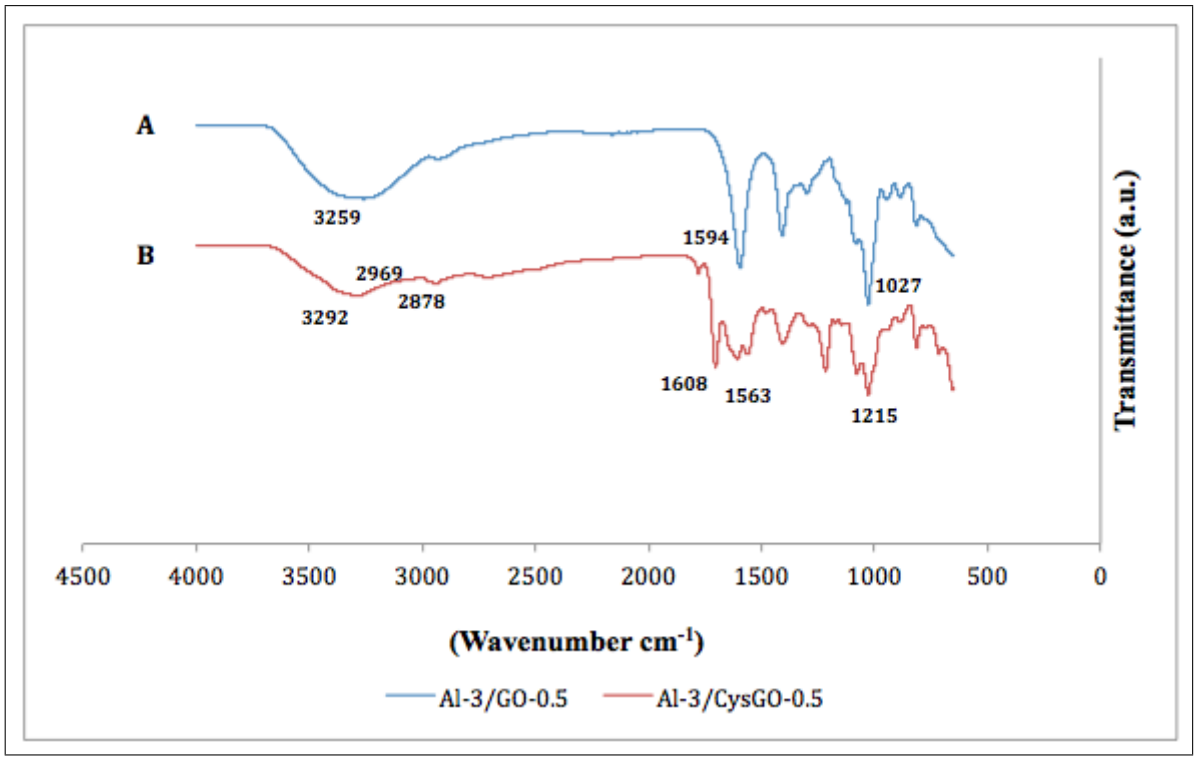

Figure 4.4 FTIR spectra of A) Al-3/GO-0.5 and B) Al-3/CysGO-0.5 experimental groups.

The FTIR analysis was conducted for Al-3/GO-0.5 and Al-3/CysGO-0.5 experimental groups in order to investigate the immobilization of L-Cysteine on GO sheets. It is observed that the intensity of the band that represents the stretching vibrations of -OH bond has decreased as expected with the addition of L-Cysteine to the structure. In the spectra of Al-3/GO-0.5, the characteristic peaks of GO such as C=C stretching mode of the sp^2 carbon skeletal network at 1497 cm^{-1} and -OH stretching vibration at 3315 cm^{-1} are visible [17].

Additional to these, peaks at 2969 cm^{-1} and 2878 cm^{-1} were observed which represent the stretching vibrations of the alkane groups introduced by L-Cysteine. The peak observed at 3292 cm^{-1} (Figure 4.4, B) corresponds to N-H stretching vibration of the amine group [90]. The peaks observed at 1563 cm^{-1} and 1215 cm^{-1} correspond to N-H bending vibration and C-N stretching vibration respectively [91]. A strong band at 1608 cm^{-1} originates from valence asymmetric vibration of C=O bond from L-cysteine [92].

4.2 Swelling Ratio

Since absorbance capacity is a key property in desired application, swelling ratios were calculated for experimental groups Al-1/GO-1, Al-2/GO-1, Al-3/GO-1, Al-3/GO-0.5, Al-3/GO-2 and Al-3/CysGO-0.5. The effect of cross linker and GO concentration and also L-Cysteine immobilization on swelling behaviour was investigated.

Figure 4.5, A and Figure 4.5, B represent the effect of cross linker concentration and the effect of GO concentration on swelling ratio, respectively. Figure 4.6 represents the effect of L-Cysteine on the swelling ratio.

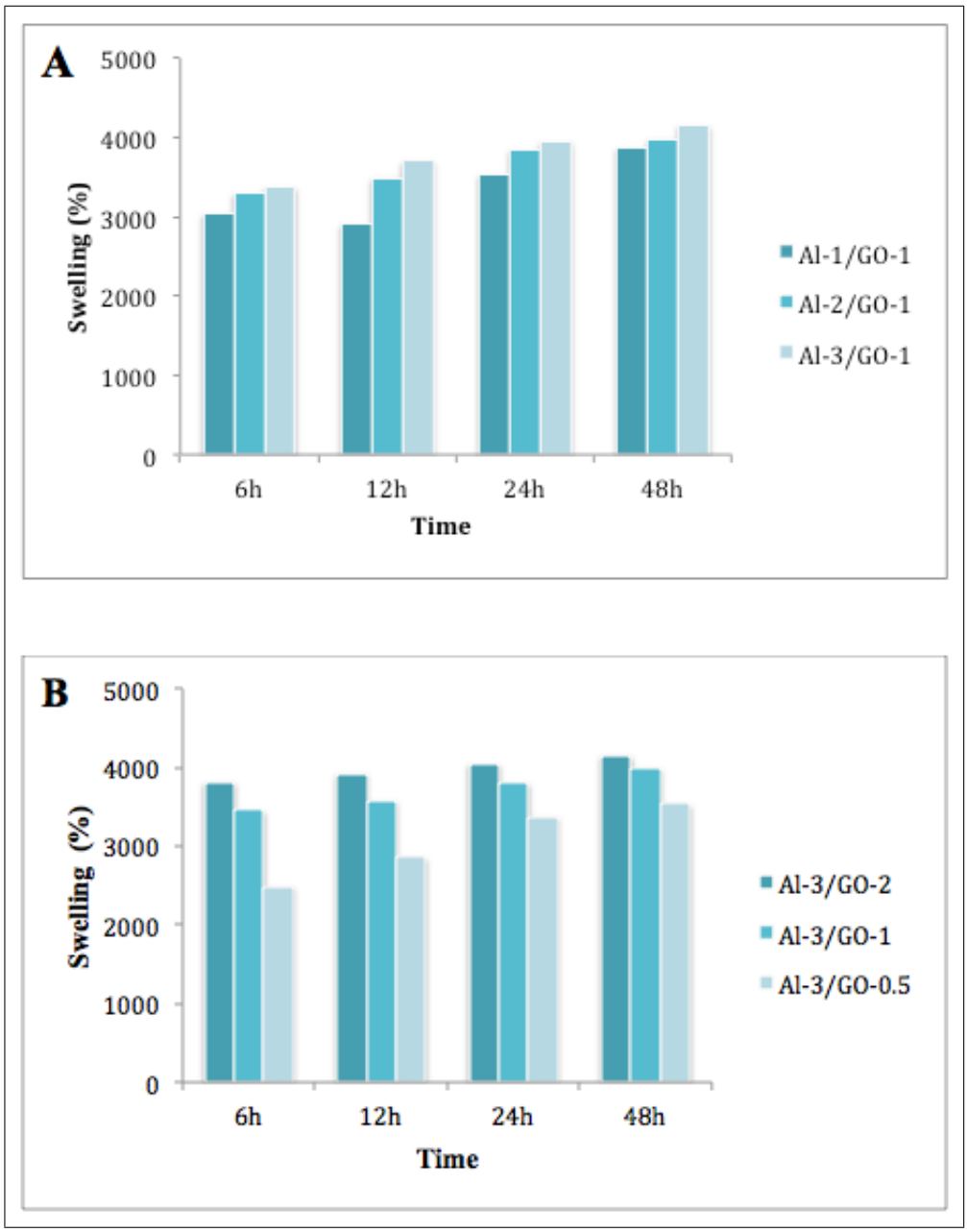

Figure 4.5 Swelling ratio of the experimental groups A) Al-1/GO-1, Al-2/GO-1 and Al-3/GO-1 with different cross linker concentration, B) Al-3/GO-0.5, Al-3/GO-1 and Al-3/GO-2 with different GO concentration.

In the first set of data (Figure 4.5, A) an increase in swelling ratio was observed with increasing cross linker concentration. For the group with lowest cross linker concentration (Al-1/GO-1), a drop occurred in the swelling ratio at the time point 12h, but continued to increase afterwards. The final (48h) swelling ratio values obtained in this work ranged between 3870-4070%.

In the second set of data (Figure 4.5, B) an increase in swelling ratio is observed with increasing GO concentration. The final (48h) swelling ratio values obtained in this work ranged between 3536-4151%.

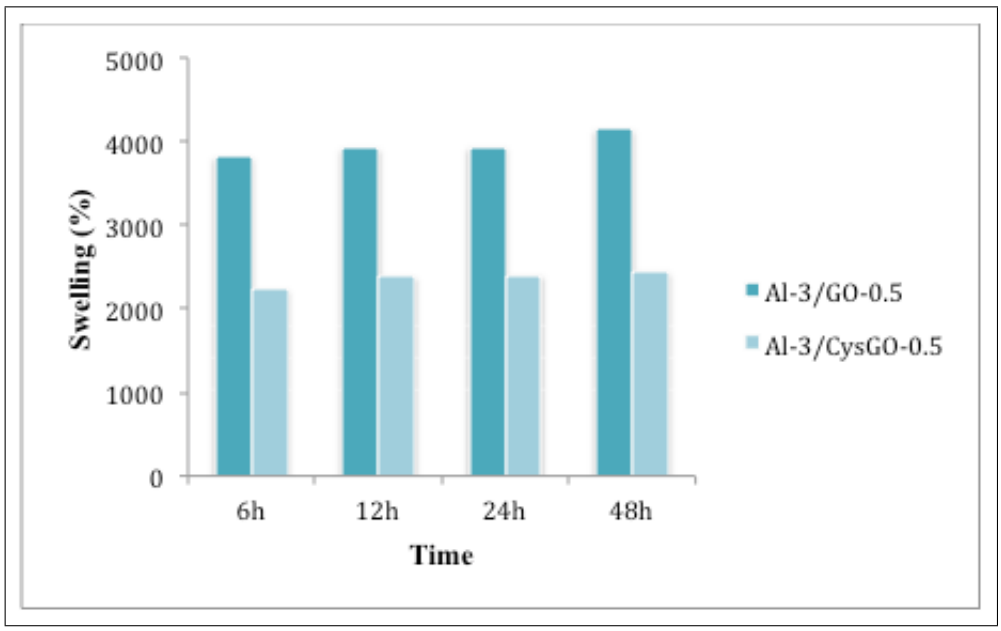

Figure 4.6 Swelling ratio of the experimental groups Al-3/GO-0.5 and Al-3/CysGO-0.5.

In the third set of data (Figure 4.6.), it is observed that with the introduction of L-Cysteine to the structure, there was a noticeable decrease in swelling ratio. The final (48h) swelling ratio values obtained in this work ranged between 2445-4151%.

4.3 Porosity

The percentage porosity of all experimental groups was investigated by conducting liquid replacement method at the end of 12h immersion of the scaffolds. The data are represented in Figure 4.7.

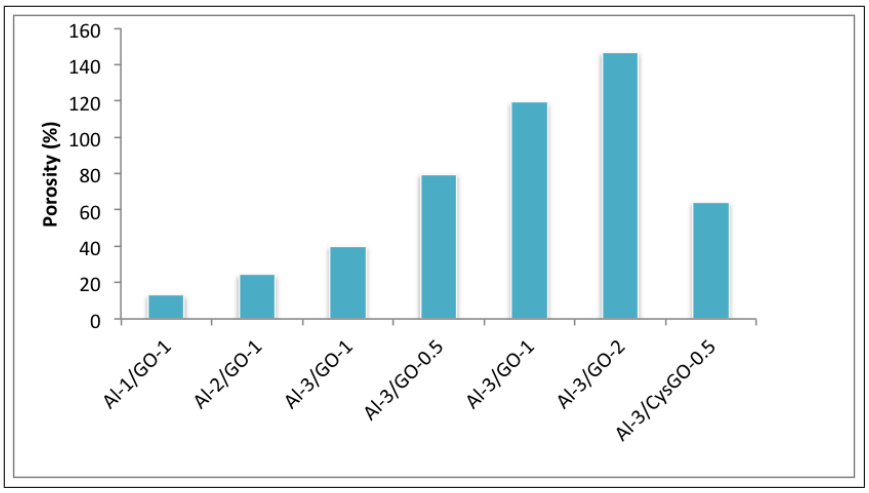

Figure 4.7 Porosity of Al-1/GO-1, Al-2/GO-1, Al-3/GO-1, Al-3/GO-0.5, Al-3/GO-1, Al-3/GO-2 and Al-3/CysGO-0.5 experimental groups.

It is observed that the higher the concentration of $CaCl_2$ leads to increase in porosity [93]. It is also observed that there is an increasing trend in porosity with increasing GO content. Introduction of L-Cysteine to the structure seems to decrease porosity. The composite scaffold with lowest cross linker concentration has the lowest porosity while the composite that has highest cross linker and GO concentration has the highest porosity.

4.4 Morphological Characterization

SEM characterization was used in order to investigate the inner morphological structure of the neat Al and Al/GO scaffolds. SEM gave an idea of interconnected porosity of the scaffolds. The SEM images of Al-3 are given in Figure 4.8 in order to demonstrate the inner structure of neat alginate scaffold with 0.03M $CaCl_2$ (Al-3). By SEM images of Al-1/GO-1, Al-2/GO-1 and Al-3/GO-1 (Figure 4.9) the effect of cross-linker concentration was investigated. By using the SEM images of Al-3/GO-0.5, Al-3/GO-1 and Al-3/GO-2 (Figure 4.10), the effect of GO concentration was investigated. SEM images of Al-3/CysGO-0.5 are also given in Figure 4.11.

Figures 4.8 to 4.11 represent Al-1, Al-2 and Al-3 (scaffolds with 0.01M, 0.02M and 0.03M $CaCl_2$, respectively) at 200x and 1000x magnification.

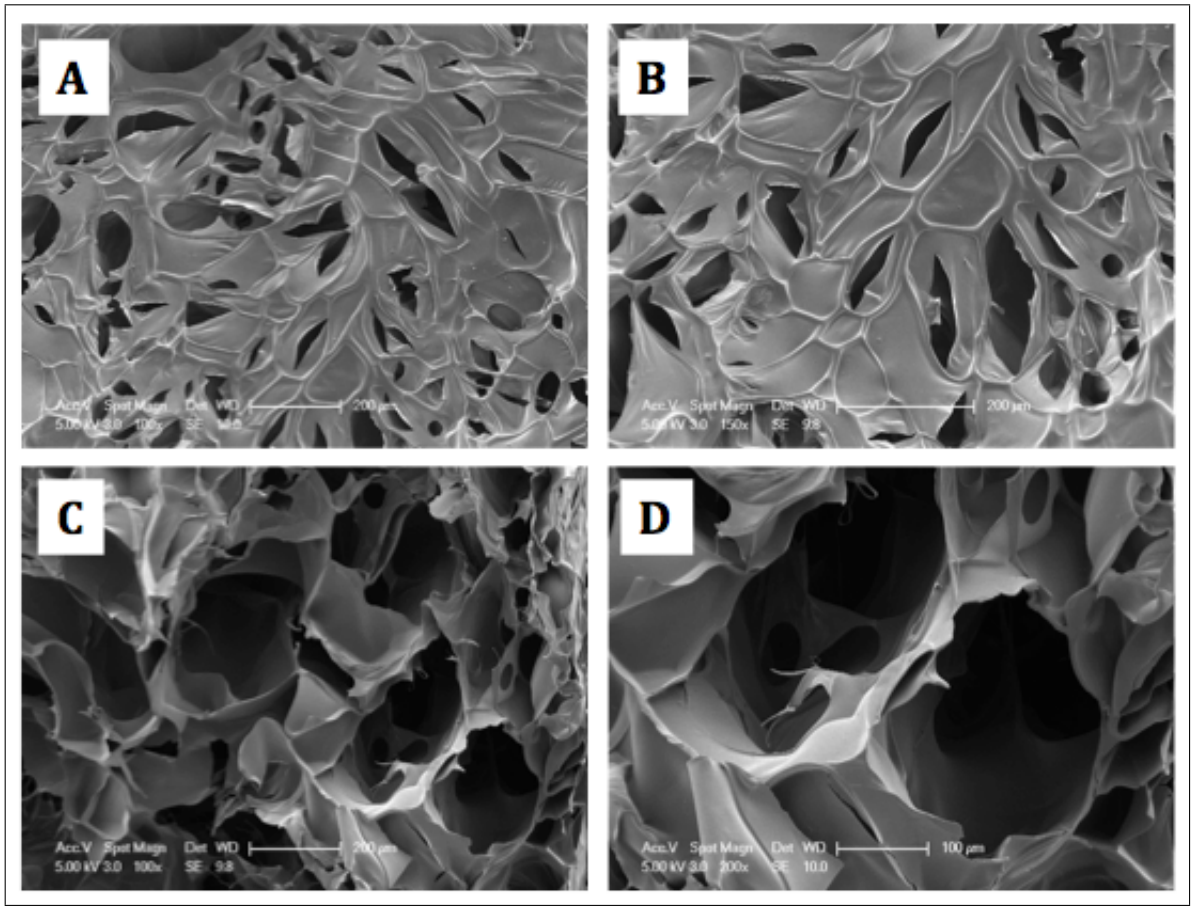

Figure 4.8 Surface (A, B) and cross section (C, D) SEM images of neat Al scaffolds with 0.03M $CaCl_2$: A) surface image at 100x, B) surface image at 150x, C) cross section image at 100x and D) cross section image at 200x.

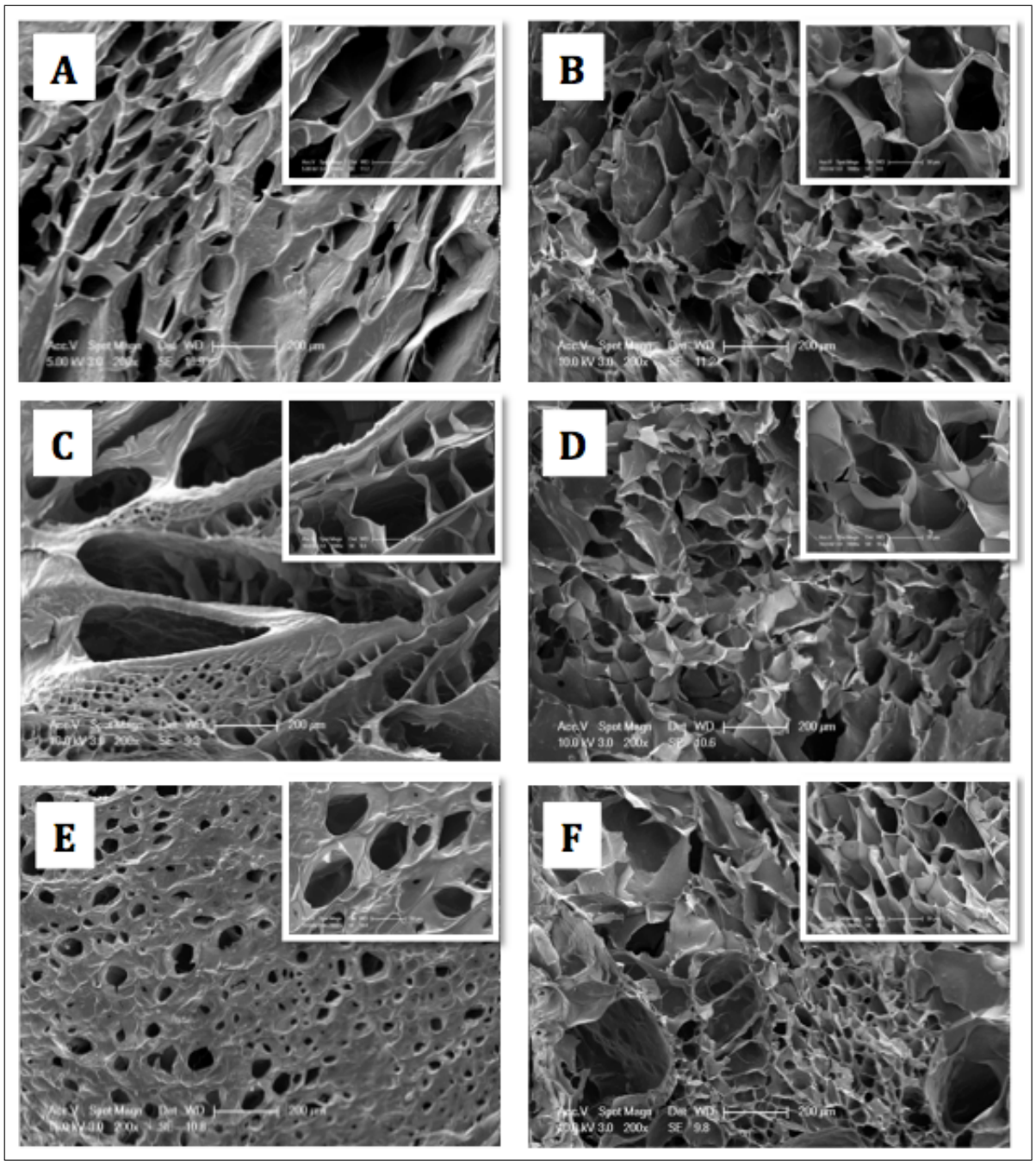

Figure 4.9 Surface (A, C, E) and cross section (B, D, F) SEM images of Al-1/GO-1 (A, B), Al-2/GO-1 (C, D), Al-3/GO-1 (E, F) at 200x with the corresponding 1000x images on the top right corner.

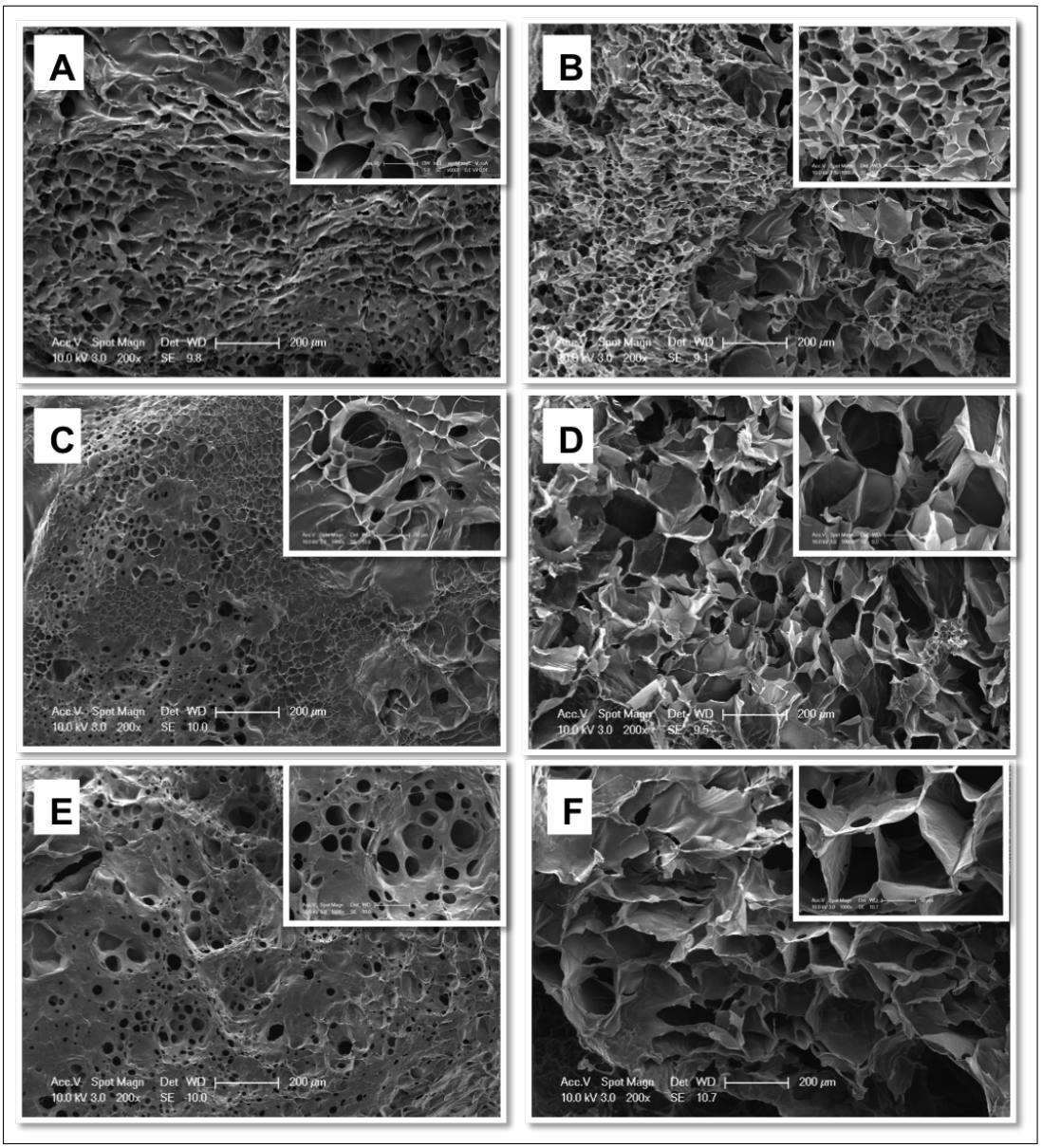

Figure 4.10 Surface (A, C, E) and cross section (B, D, F) SEM images of Al-3/GO-0.5 (A, B), Al-3/GO-1 (C, D), Al-3/GO-2 (E, F) at 200x with the corresponding 1000x images on the top right corner.

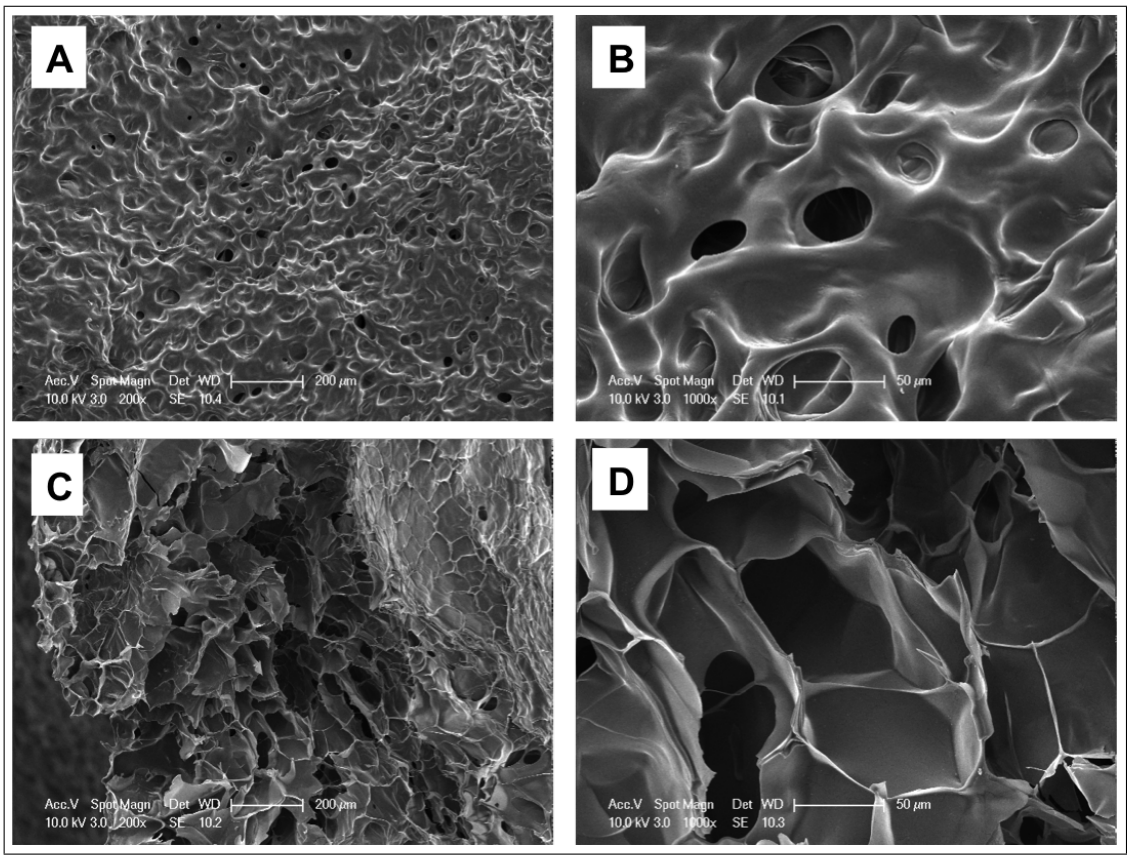

Figure 4.11 Surface (A, B) and cross section (C, D) SEM images of Al-3/CysGO-0.5 scaffold at 200x (A, C) and 1000x (B, D).

4.5 Rheological Characterization

In an effort to characterize the viscoelastic properties of neat alginate hydrogel (Al-3) and composite hydrogels with different cross linker concentrations Al-1/GO-1, Al-2/GO-1 and Al-3/GO-1 rheometry methods were employed. The data are presented in Figure 4.12, Figure 4.13 and Table 4.1.

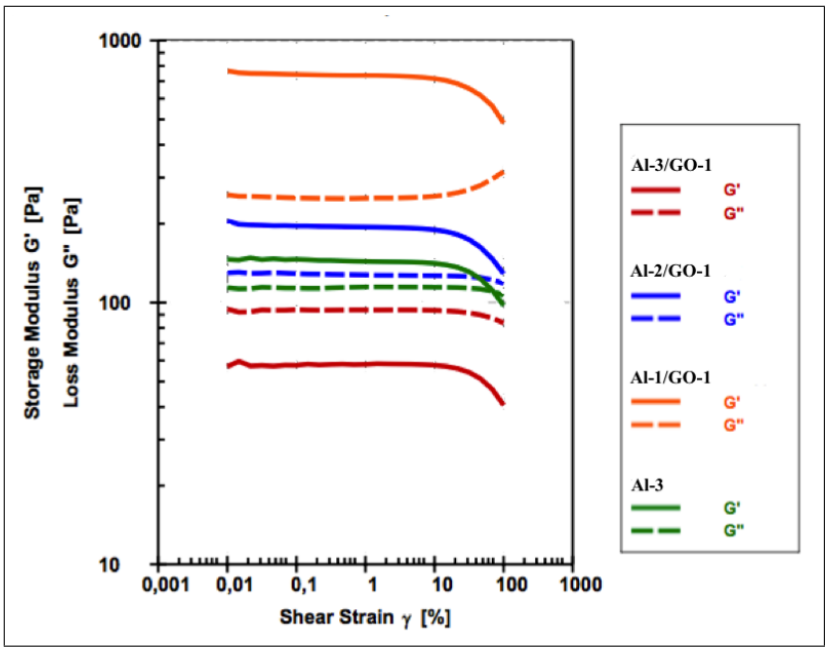

Figure 4.12 Oscillatory strain sweeps of ionically cross-linked Al and Al/GO hydrogels with different cross linker concentrations.

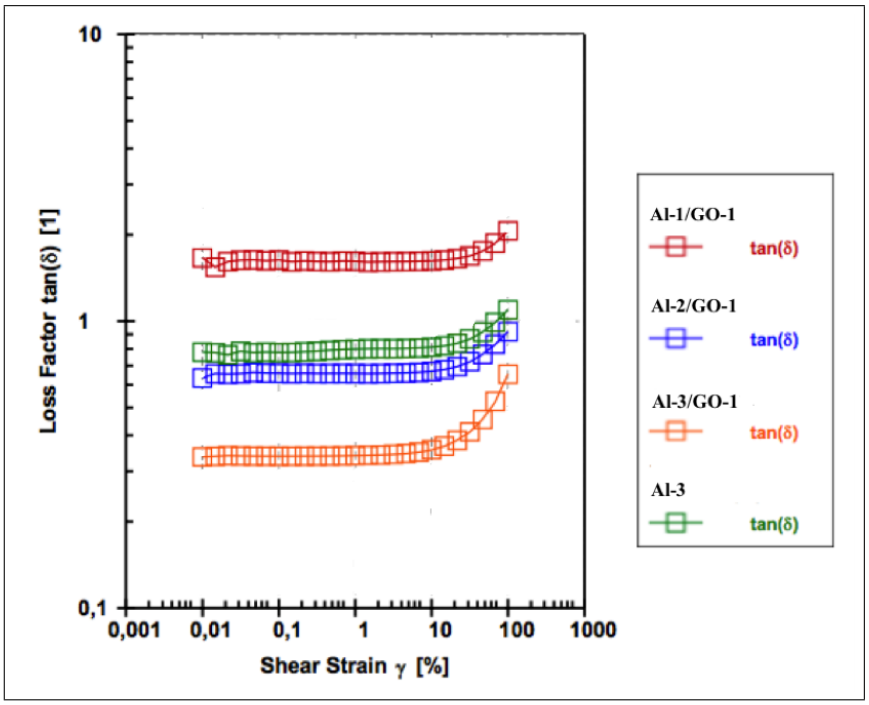

Figure 4.13 Loss factor as a function of shear strain for ionically cross-linked Al and Al/GO hydrogels with different cross linker concentrations.

The data presented in Figure 4.12 indicates that in the linear viscoelastic region while Al-1/GO-1 behaves as viscoelastic liquid (G"$>$G' and tan $\delta>1$), Al-2/GO-1, Al-3/GO-1 and Al-3 shows viscoelastic solid behavior. Among the viscoelastic solid experimental groups, Al-3/GO-1 has the highest G' value, which indicates that it has higher strength, while Al-3 has the softest structure.

According to the data presented in Figure 4.13, while Al-3, which has the highest tanδ value is the most elastic hydrogel; Al-3/GO-1 is the most brittle hydrogel. Storage modulus (G'), loss modulus (G") and tanδ values in the linear viscoelastic region are presented in Table 4.1.

Table 4.1
Storage modulus (G'), loss modulus (G") and tanδ values in the linear viscoelastic region.

	Storage Modulus [Pa]	**Loss Modulus [Pa]**	**Loss Factor [1]**
Al-1/GO-1	57.98	93.82	1.62
Al-2/GO-1	194.70	127.90	0.66
Al-3/GO-1	737.20	249.90	0.34
Al-3	144.70	113.80	0.79

4.6 Macroscopic Images

Optical images of the samples Al-3, Al-3/GO-0.5, Al-3/GO-1 and Al-3/GO-2 are presented in Figure 4.14 taken by using optical camera in order to demonstrate the color change with the addition of graphene oxide.

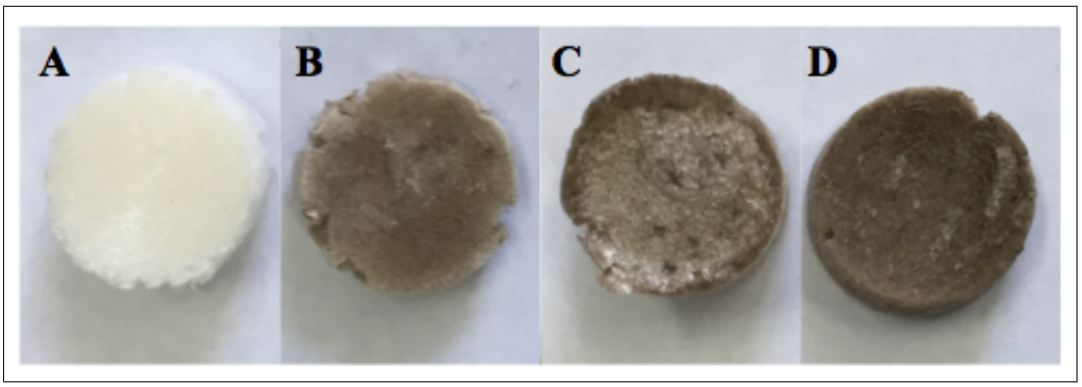

Figure 4.14 Optical images of experimental groups A) Al-3, B) Al-3/GO-0.5, C) Al-3/GO-1 and D) Al-3/GO-2.

4.7 Cell Culture Studies (MTT Assay)

The effects of cross linker concentration; GO concentration and L-Cysteine were investigated by using MTT assay. Fibroblast cells (L929-ATCC) were seeded and cultured on 96 well tissue culture plate (TCP). $1x10^4$ cells were cultured into each well (n=5 for each experimental group and control group). Then DMEM from immersed scaffolds was added into cell-cultured wells in order to evaluate the cytotoxicity of the scaffolds. MTT assay was conducted and evaluated after being incubated for 1 and 4 days.

Experimental groups that subjected to MTT assay are: Al-1/GO-1, Al-2/GO-1, Al-3/GO-1 in order to determine the optimal cross linker concentration, Al-3/GO-0.5 Al-3/GO-1 Al-3/GO-2 in order to determine the optimal GO concentration and Al-3, Al-3/CysGO-0.5 in order to demonstrate the effect of L-Cysteine immobilization and GO incorporation on cell behavior.

According to the obtained data for experimental groups Al-1/GO-1, Al-2/GO-1, Al-3/GO-1, at day 1, metabolic activity of cells were calculated and represented in Table 4.2.

Table 4.2
MTT assay results for different cross linker concentrations and TCP at day 1 (n=5). Data are expressed in means ± SD.

Experimental Group	Cell Viability (%)
Al-1/GO-1	109.00±8.94
Al-2/GO-1	112.00±5.11
Al-3/GO-1	121.00±4.09
TCP	100.00±7.93

The data suggest that at day 1 all groups exhibit higher viability compared to control group (TCP). The experimental group with the highest viability was Al-3/GO-1, while Al-1/GO-1 had the lowest viability. ANOVA was chosen as a suitable statistical method to compare and find statistical significances between experimental groups. No significant difference found between the experimental and control groups when compared to each other (df=3, F= 8,312, Sig=0,001).

The data obtained from the MTT assay at day 4 are presented in Table 4.3.

Table 4.3
MTT assay results for different cross linker concentrations and TCP at day 4 (n=5). Data are expressed in means ± SD.

Experimental Group	Cell Viability (%)
Al-1/GO-1	89.00±10.60
Al-2/GO-1	88.83±4.44
Al-3/GO-1	99.16±9.42
TCP	100.00±7.55

The data suggest that at day 4 all groups exhibit lower but sufficient viability compared to control group. The experimental group with the highest viability was Al-3/GO-1, while Al-1/GO-1 had the lowest viability. No significant difference found between the experimental and control groups when compared to each other (df=3, F=2,715, Sig=0,079). The results of day1 and day 4 are presented in Figure 4.15.

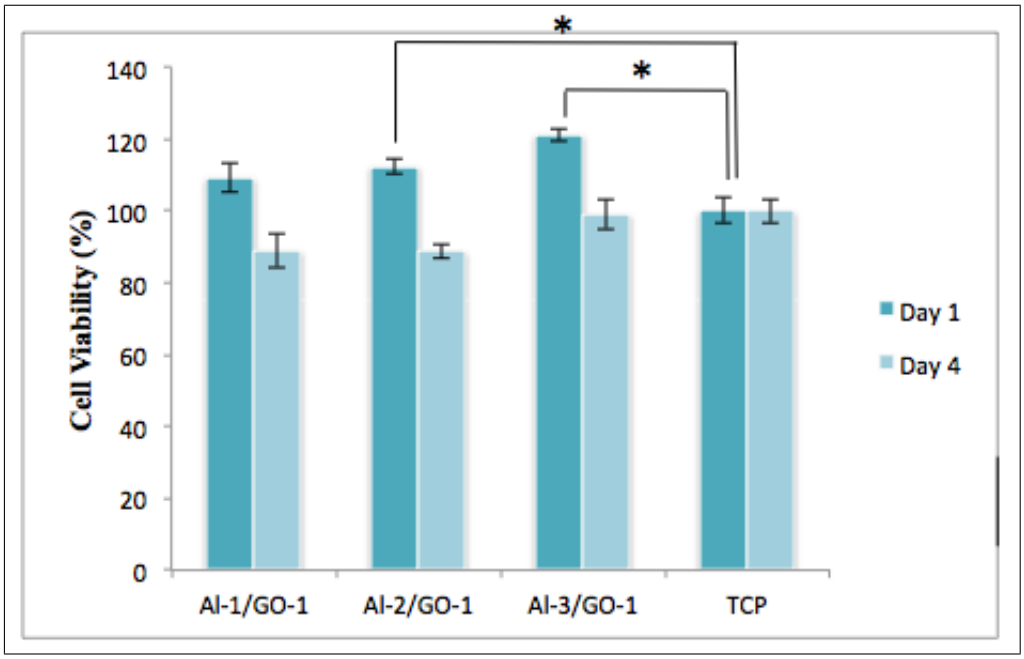

Figure 4.15 MTT assay results for different cross linker concentrations and TCP at day 1 and day 4 (n=5). Data are expressed in means ± SE and represent the results of two independent experiments.

According to the obtained data for experimental groups Al-3/GO-0.5, Al-3/GO-1, Al-3/GO-2, at day 1, metabolic activity of cells were calculated and represented in Table 4.4.

Table 4.4
MTT assay results for different GO concentrations and TCP at day 1 (n=5). Data are expressed in means ± SD.

Experimental Group	Cell Viability (%)
Al-3/GO-0.5	80.51±6.00
Al-3/GO-1	88.83±11.52
Al-3/GO-2	80.23±4.08
TCP	100.00±4.33

As shown in Table 4.4, the MTT data suggest that at day 1 all experimental groups exhibit high viability. The control group has the highest viability. Figure 4.16 indicates that at day 1 increasing GO concentration from 0.5 mg/ml to 1 mg/ml has a positive effect on cell viability. However this positive effect did not last when GO concentration was increased to 2 mg/ml, which caused a noticeable decrease in cellular activity. The control group (TCP) showed significant difference when compared to other groups (df=3,F=8,466, Sig=0,001).

The data obtained from the MTT assay at day 4 are presented in Table 4.5

Table 4.5
MTT assay results for different GO concentrations and TCP at day 4 (n=5). Data are expressed in means ± SD.

Experimental Group	Cell Viability (%)
Al-3/GO-0.5	74.64±13.21
Al-3/GO-1	57.09±7.79
Al-3/GO-2	67.45±10.02
TCP	100.00±10.33

The results of day 1 and day 4 are presented in Figure 4.16.

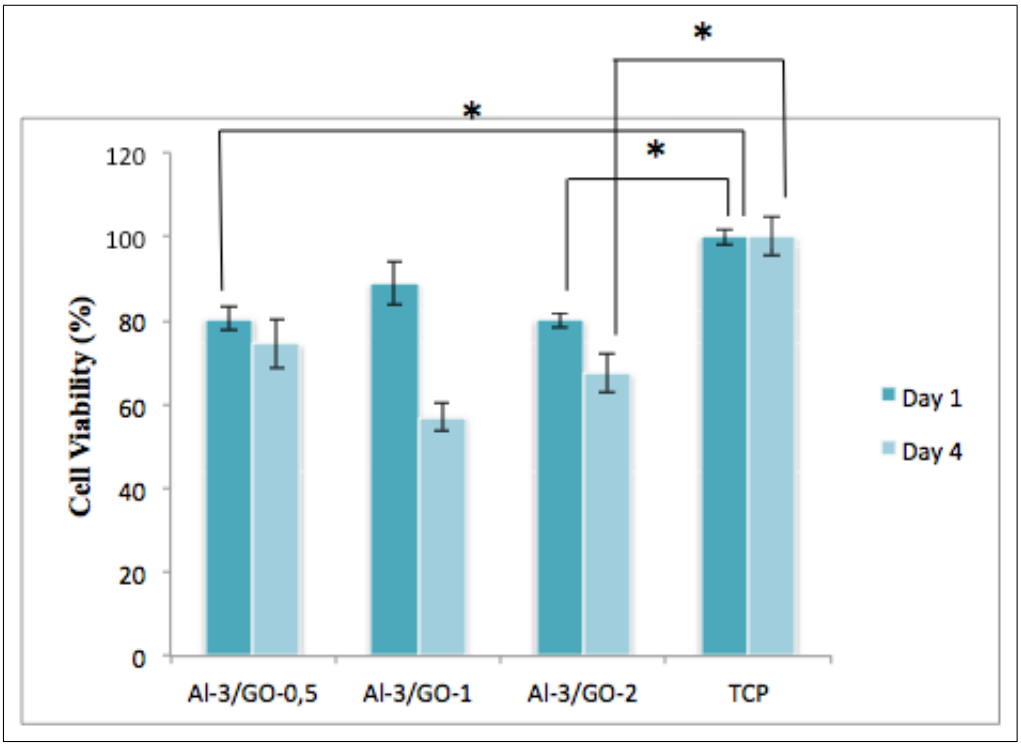

Figure 4.16 MTT assay results for different GO concentrations and TCP at day 1 and day 4 (n=5). Data are expressed in means ± SE and represent the results of two independent experiments.

As shown in Figure 4.16 cell viability decreases for all experimental groups at day 4. It is observed that the viability of Al-3/GO-1 and Al-3/GO-2 decreases considerably while the viability of Al-3/GO-0.5 decreased much less. The control group (TCP) showed significant difference when compared to other groups (df=3,F=15,095, Sig=0,000).

According to the data obtained for experimental groups Al-3, Al-3/CysGO-0.5, and control group at day 1, metabolic activity of cells were calculated and represented in Table 4.6.

Table 4.6
MTT assay results for experimental groups Al-3, Al-3/CysGO-0.5, and control group concentrations at day 1 (n=5). Data are expressed in means ± SD.

Experimental Group	Cell Viability (%)
Al-3	84.21±4.14
Al-3/CysGO-0.5	98.79±12.00
TCP	100.00±7.16

As shown in Table 4.6, the MTT data suggest that at day 1 all experimental groups exhibit high viability. An increase in viability is noticeable with GO and Cys addition. The experimental group of neat Al-3 has the lowest viability when compared to Al-3/CysGO-0.5 and control groups. The Al-3/CysGO-0.5, and control groups exhibit significant difference when compared to Al-3 group (df=3, F=5,432, Sig.0,021).

The data obtained from the MTT assay at day 4 are presented in Table 4.7.

Table 4.7
MTT assay results for experimental groups Al-3, Al-3/CysGO-0.5, and control group concentrations at day 4 (n=5). Data are expressed in means ± SD.

Experimental Group	Cell Viability (%)
Al-3	90.74±5.22
Al-3/CysGO-0.5	98.18±2.11
TCP	100.00±4.39

According to the MTT results presented in Table 4.7 and Figure 4.17, all experimental groups exhibit high viability. The group Al-3 has lower viability when compared to other groups Al-3/CysGO-0.5 and control groups have no significant difference of viability. The Al-3/CysGO-0.5, and control groups exhibit significant difference when compared to Al-3 group. (df=2, F=7,057, Sig.=0,009). The results of day 1 and day 4 are presented in Figure 4.17.

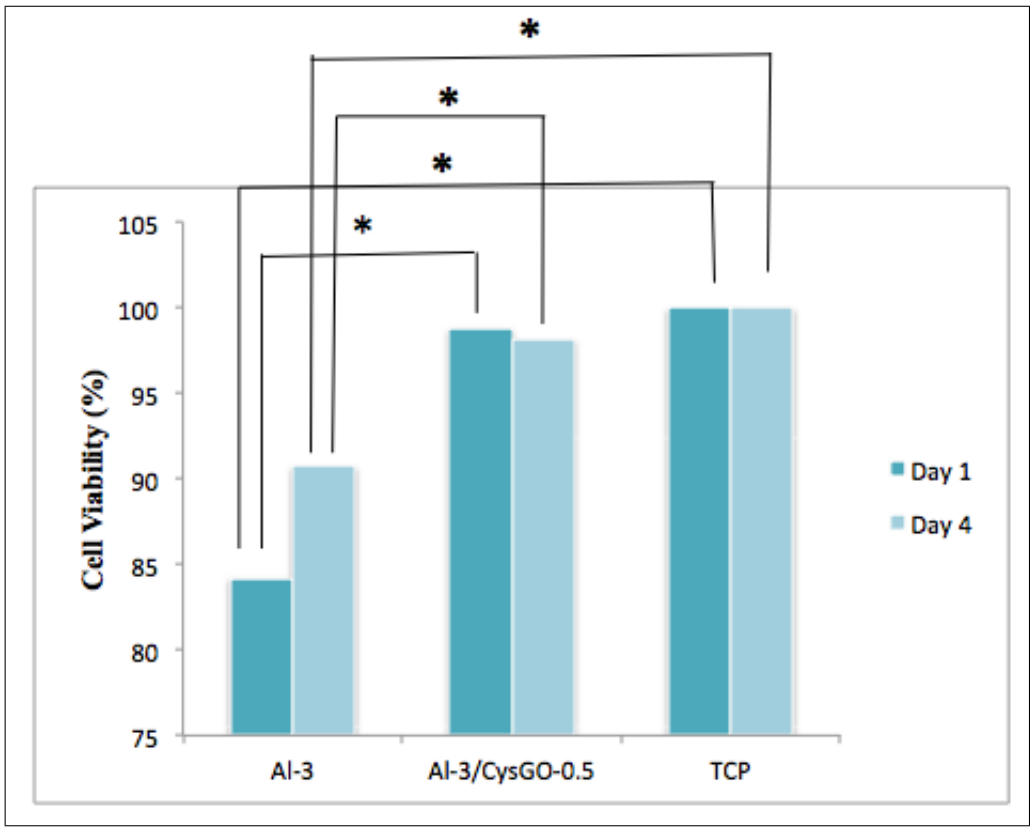

Figure 4.17 MTT assay results for experimental groups Al-3, Al-3/CysGO-0.5, and control group at day 1 and day 4 (n=5). Data are expressed in means ± SE and represent the results of two independent experiments.

5. DISCUSSION

Alginate (Al) as a natural polymer is widely used as wound care material owing to its favourable properties such as biocompatibility, high absorbency and facility of gelation [12, 13] However, alginate has some deficiencies such as poor mechanical strength, uncontrollable degradation and loss of structural integrity that may limit its application as a biomaterial [94].

In this thesis, alginate/graphene oxide composite 3D porous scaffolds were fabricated and characterized with the purpose of achieving a material suitable for wound care and healing applications with enhanced properties such as biocompatibility, high mechanical strength, stability, high absorbance and positive cell response. The effect of cross linker ($CaCl_2$) and graphene oxide (GO) concentration and L-Cysteine immobilization was investigated along with characterization techniques such as FTIR, swelling ratio, porosity, SEM, Rheometry. In addition MTT assay was conducted in order to investigate cell viability.

5.1 Fourier Transform Infrared (FTIR) Spectroscopy

In order to investigate the chemical structure and determine the interactions and the intermolecular bonds between alginate/$CaCl_2$, alginate/GO and GO/L-Cysteine, FTIR analysis was conducted. FTIR analysis is an easy method used to identify the presence of certain functional groups in a molecule.

Alginate has several functional groups such as hydroxyl (-OH) and carboxylic groups (-COOH) and intermolecular bonds such as C-H, C-O-C and C-O bonds as shown in Figure 2.3.

As illustrated in Figure 4.1 (A), the spectrum of alginate presents stretching

vibrations of -OH bonds can be observed in the range of 3200 cm^{-1} - 3400 cm^{-1}. And stretching vibrations of aliphatic C-H can be observed at 2926 cm^{-1}. Dominant absorption bands at 1595 cm^{-1}, and 1405 cm^{-1} refer to asymmetric and symmetric stretching vibration of carboxylate salt group respectively.

It is known that alginate goes under gelation process when in the presence of divalent cations [51]. In order to obtain an ionically crosslinked gel $CaCl_2$ solution was added to the alginate powder. With the addition of $CaCl_2$ (Figure 4.1, (B, C, D)) peak shifts observed from 1595 cm^{-1} to 1593 cm^{-1} and also from 1405 cm^{-1} to 1409 cm^{-1}. These shifts appear as the result of the replacement of Na^+ in the guluronic acid residues and Ca^{2+} cation, therefore change of charge density and radius of the atomic weight of the cation [95]. This indicates the involvement of the COO- group in the alginate reticulation process and formation of egg box structure through Ca^{2+} [96]. Also band of stretching vibrations of O-H bonds in cross linked alginate appeared narrower than neat alginate due to the involvement of carboxylate and hydroxyl groups of alginate to the Ca^{2+} [95]. The data suggest that the gelation of alginate via cross linker $CaCl_2$ was successfully done.

Figure 4.2 presents the FTIR spectra of neat alginate and alginate/GO composite scaffolds with different $CaCl_2$ concentrations (0.01M, 0.02M, 0.03M). An increase in the intensity of the band that corresponds to the stretching vibrations of -OH bond was observed compared to neat alginate spectrum. Also, -OH absorption bands widened slightly and mildly shifted to lower wavenumbers (0.01M= from 3281 cm^{-1} to 3265 cm^{-1}; 0.02M= from 3331 $cm^{-1}$to 3296 cm^{-1}; 0.03M= from 3272 $cm^{-1}$to 3254 cm^{-1}) as a result of the interaction of sodium alginate and GO via intermolecular H bonds [17, 60]. The data verify the integration of GO to the alginate structure.

FTIR spectra of samples Al-3, Al-3/GO-0.5, Al-3/GO-1 and Al-3/GO-2 with different GO concentrations were also recorded and compared as shown in Figure 4.3. It is observed that the intensity of the -OH stretching vibration peak heightens as the concentration of GO increases. GO is very abundant of -OH functional group, therefore it is expected that the higher the GO content, the greater the intensity -OH stretching

vibration peak. Furthermore a slight red shift (increase in wavelength) was observed in the same band, which affirms the interfacial adhesion and hydrogen bonding (Figure 3.2) between alginate and GO [17, 89].

The FTIR spectrum of the composite scaffolds with addition of L-Cysteine is presented in Figure 4.4. The intensity of the band that represents the stretching vibrations of -OH bond has decreased as expected due to binding of L-Cysteine to the -OH group of GO. The characteristic peaks of GO such as C=C stretching mode of the sp^2 carbon skeletal network at 1497 cm^{-1} and -OH stretching vibration at 3315 cm^{-1} are observable [17]. Furthermore, the stretching vibrations of the alkane groups introduced by L-Cysteine are present at the 2969 and 2878 cm^{-1} peaks. Also, characteristic peaks of L-Cysteine such as N-H bending vibration, C-N stretching vibration and valence asymmetric vibration of C=O bond are observed at 1563,1215 and 1608 cm^{-1}, correspondingly [91, 92]. The data indicate that L-Cysteine was successfully immobilized on GO sheets.

5.2 Swelling Ratio

The liquid absorbance capacity is an important parameter in desired application. Alginate is known for its high absorbance. This property makes it preferable for high exudate wounds. The high absorption property limits wound exudations and reduces bacterial contamination [1].

In order to investigate the absorbance capacity of the fabricated samples, the swelling test was performed for all composite groups. The samples were immersed in DMEM medium in order to get additional information on absorbance and stability of the scaffolds in cell friendly environment compared to DI water. The time points were 6h, 12h, 24h and 48h. The effect of cross linker and GO concentration and also L-Cysteine immobilization on swelling behaviour was investigated.

As presented in Figure 4.5 (A), the swelling ratio increased with the increasing cross linker content. The experimental group with the lowest cross linker content experiences a drop in swelling ratio at 12h. This decrease is due to the solubility of the uncross-linked alginate because of the nonsufficient cross-linker content. Likewise, the highest swelling ratio belongs to the experimental group with the highest cross linker content because of the small amount of uncross-linked alginate.

The data in Figure 4.5 (B) shows that the swelling ratio increases as the GO content increase. Since GO is abundant of hydrophilic functional groups such as carboxyl and hydroxyl ready to form H bonds [97].

As seen in Figure 4.6 swelling ratio lowers with the addition of L-Cysteine to the scaffold structure. Since L-Cysteine is a hydrophobic amino acid, the decrease in the swelling capacity is expected.

5.3 Porosity

The porous structure of the scaffolds was accomplished by using freeze-drying method as the fabrication method of the scaffolds. Freeze drying is a procedure by which the samples are frozen in a cold environment and then the frozen contents are removed via sublimation under high vacuum, resulting in formation of porous structures [98]. Porosity is a critical aspect in 3D scaffolds. Therefore the porosity of the composite scaffolds was investigated by conducting liquid replacement method. The data presented in Figure 4.7 indicates that cross linker concentration has an effect on porosity. The porosity of groups Al-3/GO-1 and Al-3/GO-2 was higher that 100% due to ionic interaction and amino acid salt accumulation that comes from the ingredients of DMEM media. It is observed that porosity increases by increasing cross linker content. The higher concentration of $CaCl_2$ gives rise to more junction zones and increases number of pores number [93]. It can be seen that porosity increases with the increasing GO content. Since the porosity was measured via liquid replacement method, the observed increase in porosity with increasing GO content may be

due to high absorbance capacity with increasing GO content. The data also showed that introduction of L-Cysteine to the structure lowers porosity and likewise it may be the result of decreasing absorbance capacity resulted by the hydrophobic nature of the amino acid. In order to obtain further information about porosity, SEM images of the samples were investigated.

5.4 Morphological Characterization

The morphology of neat alginate and alginate/GO composite scaffolds was observed with SEM imaging. In order to have supplementary data on porosity, SEM images of both surface and cross section of the scaffolds were taken. The SEM images provided more precise information about the porous structure of the scaffolds.

Figure 4.8 presents the SEM images of neat alginate scaffolds (Al-3). In Figure 4.8 (A, B) the open and closed pores on the surface are visible. The pore walls are highly distinct. In Figure 4.8 (C, D) it is observed that the Al -3 scaffolds exhibit highly porous and interconnected structure as expected. In Figure 4.9 the SEM images of scaffolds with different $CaCl_2$ concentrations are presented. It is observed that the inner structure and porosity does not differ significantly as seen in the cross section images given in Figure 4.9 (B, D, F). The SEM data indicates that incorporation of $CaCl_2$ causes no detrimental effect on highly porous and interconnected structure of the alginate/GO composite scaffolds [17].

In Figure 4.10 the effect of GO content on porous structure is demonstrated through SEM images of the experimental groups Al-3/GO-0.5, Al-3/GO-1 and Al-3/GO-2. It is observed that as the GO content increases the pore walls become less distinct on the surface and a smoother superficial structure is observed. Also the data indicate that the pores seem to get smaller with the increasing GO content due to compaction of the structure with interaction between alginate and GO (Figure 4.10 A, C, E) [17].

Figure 4.11 presents the SEM images of L-Cysteine immobilized scaffolds (Al-3/CysGO-0.5). A relatively smoother surface with smaller and less distinct pores was observed. The cross section images imply that L-Cysteine immobilization has no damaging effect on the interconnected porous structure of the scaffolds.

5.5 Rheometry

In order to investigate the viscoelastic properties of the non-lyophilized neat alginate hydrogel (Al-3) and composite hydrogels with different cross linker concentrations Al-1/GO-1, Al-2/GO-1 and Al-3/GO-1 rheometry methods were employed. The effects of GO and cross linker concentration on viscoelasticity of the hydrogels were studied.

Parameters such as the loss modulus (G"), which describes the viscous properties, the storage modulus (G'), which describes the elastic properties and loss factor (tanδ= G"/ G') were measured in order to understand the viscoelastic behaviour of the hydrogels.

The data presented in Figure 4.11 indicates that in the linear viscoelastic region while Al-1/GO-1 behaves as viscoelastic liquid (G">G' and tan δ>1), Al-2/GO-1, Al-3/GO-1 and Al-3 exhibits viscoelastic solid behavior. This indicates that low cross linker content results in low gelation, thus less rigid structure. Among the viscoelastic solid experimental groups, while Al-3/GO-1 has the highest G' value, which indicates that it has higher strength; Al-3 has the softest structure thus lower strength. This difference indicates that incorporation of GO to the structure provides stiffness to the hydrogel, consequently enhances its mechanical strength. The data given in Figure 4.12 imply that Al-3, which has the highest tanδ value, is the most elastic hydrogel; Al-3/GO-1 is the most brittle hydrogel, due to incorporation of GO to the structure.

5.6 Macroscopic Images

Figure 4.13 presents the macroscopic images of Al-3, Al-3/GO-0.5, Al-3/GO-1 and Al-3/GO-2 experimental groups. The images reveal that neat alginate scaffold presents white colour, while alginate/GO scaffolds are brown and the colour becomes darker with the increasing GO content.

5.7 Cell Culture Studies (MTT Assay)

Firstly the effect of cross linker concentration on fibroblast cell (L929, ATC, USA) viability was investigated on experimental groups Al-1/GO-1, Al-2/GO-1, Al-3/GO-1 at day 1 and day 4. According o Table 4.2, and Figure 4.14 at day 1 while all experimental groups exhibit higher viability compared to control group (TCP), Al-3/GO-1, which was the group with the highest cross linker concentration showed the highest viability. However ANOVA test showed no significant difference between groups.

At day 4, all groups exhibit lower but sufficient viability compared to control group. ANOVA test showed no significant difference between groups. Yet Al-3/GO-1, which was the group with highest cross linker concentration kept showing the highest viability among the experimental groups. This may be caused by the dissolution of the un-crosslinked alginate in case of low cross linker concentration. The experimental group with the highest viability, which is the Al-3/GO-1, was selected as the optimal cross linker concentration for proceeding with the next stage of the study.

Next, the effect of GO concentration on fibroblast cell (L929, ATC, USA) viability was investigated on experimental groups Al-3/GO-0.5, Al-3/GO-1, Al-3/GO-2 at day 1 and day 4. According to the results of MTT assay which are presented in Table 4.4, and Figure 4.15; at day 1, TCP that was the control group, showed highest cellular activity whereas the experimental groups also exhibited high viability. Accord-

ing to ANOVA, TCP showed significant difference when compared to other groups. The data indicate that increasing GO concentration from 0.5 mg/ml to 1 mg/ml has a positive effect on cell viability. However this positive effect did not last when GO concentration was increased to 2 mg/ml, which caused a noticeable decrease in cellular activity indicating that cells do not respond well to higher concentrations of GO.

As shown in Table 4.5 and Figure 4.15, at day 4, it was observed that the viability of Al-3/GO-1 and Al-3/GO-2 decreases considerably while the viability of Al-3/GO-0.5 decreased also but not as critically. The decrease in viability for the groups Al-3/GO-1 and Al-3/GO-2 corroborates the theory that cells do not respond well to high GO concentrations due to can cause a dose-dependent oxidative stress in cells [18]. From this point of view, Al-3/GO-0.5, which was the experimental group with the lowest GO concentration, was selected for the optimal GO concentration for proceeding with the next stage of the study.

As the final step, the effect of L-Cysteine and GO incorporation to the alginate scaffolds on fibroblast cell viability was investigated on experimental groups Al-3/CysGO-0.5 and Al-3. The results for MTT assay at day 1 are presented in Table 4.6 and Figure 4.16. The data suggest that at day 1 all experimental groups exhibit high viability, in addition, an increase in viability is noticeable with GO and L-Cysteine addition. According to ANOVA, the Al-3/CysGO-0.5, and control groups exhibit significant difference when compared to Al-3 group.

As shown in Table 4.7 and Figure 4.16, all groups show high viability also at day 4, Al-3 has lower viability when compared to other groups while Al- 3/CysGO-0.5 and control groups have no significant difference. Statistical analysis detected significant difference between Al- 3/CysGO-0.5 and Al-3, and TCP and Al-3. The data indicate that incorporation of GO and L-Cysteine to the structure results in positive cell response and high viability.

In the literature, there are no cell studies performed on alginate/graphene oxide composite scaffolds to the best of our knowledge. However, J. Ciriza et al. reported

that the viability of encapsulated C2C12 myoblast cells with alginate microcapsules GO was increased compared to no GO incorporation when used in small amounts [99]. The data presented in part 4.7 also suggested that although cell viability increases with the introduction of GO, increasing the GO concentration has negative effect on cell viability. Eiselt et. al reported that fibroblasts showed high viability and uniform distribution in porous alginate beads modified with RGD peptide [96]. Spitzer et. al. reported that they found significantly higher cell response and proliferation with chrondocytes in the composite alginate-fibrin beads when compared to neat alginate beads [100]. Çelik et. al. reported that with high crosslinker concentration on alginate/ Fmoc-diphenylalanine hydrogel networks, viability decreases due to inadequate growth space and denser environment for cells. This thesis has shown to eliminate this negative side effect by performing indirect MTT. In the same study it is also reported that storage modulus (G') increased with increasing cross linker ($CaCl_2$) concentration, enhancing the mechanical property [101]. This expected increase could also be seen in the rheological evaluation presented in part 4.5. Kawaguchi et. al. reported that the incorporation of CNTs into alginate gel enhanced the mechanical property compared to neat alginate gels' without affecting the original microstructure [61]. According to the data presented in part 4.5 we also achieved to enhance the mechanical property by adding GO instead of CNTs, which is known to have poor solubility and toxic impurities [17].

5.8 Future Studies

In this thesis, the results of characterization and cell studies supported that incorporation of GO and GO and L-Cysteine to the alginate structure is a promising method to achieve an enhanced biomaterial for use in wound healing applications. In further studies, antimicrobial activity will be evaluated and immobilization of several other amino acids such as L-Tryptophan on GO will be investigated in order to have additional information about the possible improvements in the scaffold properties and their effects on different cell behaviour by using keratinocytes.

REFERENCES

1. Boateng, J., and O. Catanzano, "Advanced Therapeutic Dressings for Effective Wound Healing - A Review," *Journal of Pharmaceutical Sciences*, Vol. 104, no. 11, pp. 3653–3680, 2015.

2. Vasquez, J. A., and D. H. Keast, "Contemporary issues in wound infection managing the risks, treating the problem," *Wounds*, no. November, 2006.

3. Wu, S. C., W. Marston, and D. G. Armstrong, "Wound care: The role of advanced wound healing technologies," *Journal of Vascular Surgery*, Vol. 52, no. 3 SUPPL., pp. 59S–66S, 2010.

4. Bueno, C. Z., A. M. A. Dias, H. J. C. De Sousa, M. E. M. Braga, and Â. M. Moraes, "Control of the properties of porous chitosan-alginate membranes through the addition of different proportions of Pluronic F68," *Materials Science and Engineering C*, Vol. 44, pp. 117–125, 2014.

5. Ribeiro, A. J. a. M., A. C. Gomes, and A. M. Cavaco-Paulo, "Developing scaffolds for tissue engineering using the Ca2+-induced cold gelation by an experimental design approach.," *Journal of biomedical materials research. Part B, Applied biomaterials*, Vol. 100, no. 8, pp. 2269–78, 2012.

6. Burke, J. F., I. V. Yannas, W. C. Quinby, C. C. Bondoc, and W. K. Jung, "Successful use of a physiologically acceptable artificial skin in the treatment of extensive burn injury.," *Annals of surgery*, Vol. 194, no. 4, p. 413, 1981.

7. Mayol, L., D. De Stefano, V. Campani, F. De Falco, E. Ferrari, C. Cencetti, P. Matricardi, L. Maiuri, R. Carnuccio, A. Gallo, M. C. Maiuri, and G. De Rosa, "Design and characterization of a chitosan physical gel promoting wound healing in mice," 2014.

8. Sandoval, M., C. Albornoz, S. Muñoz, M. Fica, I. García-Huidobro, R. Mertens, and A. Hasson, "Addition of chitosan may improve the treatment efficacy of triple bandage and compression in the treatment of venous leg ulcers.," *Journal of drugs in dermatology*, Vol. 10, no. 1, pp. 75–79, 2011.

9. Chou, T. C., E. Fu, C. J. Wu, and J. H. Yeh, "Chitosan enhances platelet adhesion and aggregation," *Biochemical and Biophysical Research Communications*, Vol. 302, no. 3, pp. 480–483, 2003.

10. Okamoto, Y., R. Yano, K. Miyatake, I. Tomohiro, Y. Shigemasa, and S. Minami, "Effects of chitin and chitosan on blood coagulation," 2003.

11. Khan, F., and S. R. Ahmad, "Polysaccharides and Their Derivatives for Versatile Tissue Engineering Application," *Macromolecular Bioscience*, Vol. 13, no. 4, pp. 395–421, 2013.

12. Lee, K. Y., and D. J. Mooney, "Alginate : properties and biomedical applications," *Progress in Polymer Science*, Vol. 37, no. 1, pp. 106–126, 2013.

13. Fan, J., Z. Shi, M. Lian, H. Li, and J. Yin, "Mechanically strong graphene oxide/sodium alginate/polyacrylamide nanocomposite hydrogel with improved dye adsorption capacity," *Journal of Materials Chemistry A*, Vol. 1, no. 25, p. 7433, 2013.

14. Dickinson, L. E., and S. Gerecht, "Engineered biopolymeric scaffolds for chronic wound healing," *Frontiers in Physiology*, Vol. 7, no. AUG, 2016.

15. Sweeney, I. R., M. Miraftab, and G. Collyer, "A critical review of modern and emerging absorbent dressings used to treat exuding wounds," 2012.

16. Pirone LA, Bolton LL, Monte KA, S. R., "Effect of calcium alginate dressings on partial-thickness wounds in swine," 1992.

17. Wan, Y., X. Chen, G. Xiong, R. Guo, and H. Luo, "Synthesis and characterization of three-dimensional porous graphene oxide/sodium alginate scaffolds with enhanced mechanical properties," *Materials Express*, Vol. 4, no. 5, pp. 429–434, 2014.

18. Chang, Y., S.-T. Yang, J.-H. Liu, E. Dong, Y. Wang, A. Cao, Y. Liu, and H. Wang, "In vitro toxicity evaluation of graphene oxide on A549 cells," *Toxicology Letters*, Vol. 200, no. 3, pp. 201–210, 2011.

19. Liao, K. H., Y. S. Lin, C. W. MacOsko, and C. L. Haynes, "Cytotoxicity of graphene oxide and graphene in human erythrocytes and skin fibroblasts," *ACS Applied Materials and Interfaces*, Vol. 3, no. 7, pp. 2607–2615, 2011.

20. Georgakilas, V., M. Otyepka, A. B. Bourlinos, V. Chandra, N. Kim, K. C. Kemp, P. Hobza, R. Zboril, and K. S. Kim, "Functionalization of graphene: covalent and non-covalent approaches, derivatives and applications," *Chemical Reviews*, Vol. 112, no. 11, pp. 6156–6214, 2012.

21. Maleki, N., A. Safavi, F. Sedaghati, and F. Tajabadi, "Efficient electrocatalysis of l-cysteine oxidation at carbon ionic liquid electrode," 2007.

22. Bouri, M., R. Salghi, A. Ríos, and M. Zougagh, "Fluorescence Determination of L-Cysteine in Wound Dressings by Fluoroscein Coated Gold Nanoparticles," *Analytical Letters*, Vol. 2719, no. August, p. 00032719.2015.1098655, 2015.

23. Monlar, J. A., ed., *Nutrition and Wound Healing*, CRC Press, 2006.

24. Enoch, S., and D. J. Leaper, "Basic science of wound healing," *Surgery*, Vol. 26, no. 2, pp. 31–37, 2007.

25. Sezer, A. D., and E. Cevher, "Biopolymers as Wound Healing Materials: Challenges and New Strategies," *Biomaterials Applications for Nanomedicine*, pp. 383–414, 1992.

26. Mutsaers, S. E., J. E. Bishop, G. McGrouther, and G. J. Laurent, "Mechanisms of tissue repair: from wound healing to fibrosis," *The international journal of biochemistry and cell biology*, Vol. 29, no. 1, pp. 5–17, 1997.

27. Clark, M., "Rediscovering alginate dressings," *Wounds International*, Vol. 3, no. 1, pp. 3–6, 2012.

28. Piraino, F., and Š. Selimović, "A Current View of Functional Biomaterials for Wound Care, Molecular and Cellular Therapies," *BioMed Research International*, Vol. 2015, 2015.

29. Watson, T., "Soft Tissue Repair and Healing Review Introduction," *Soft Tissue Healing*, 2014.

30. Paul, W., and C. P. Sharma, "Advances in Wound Healing Materials : Science and Skin Engineering," *Advances in Wound Healing Materials : Science and Skin Engineering*, no. June, p. 296, 2015.

31. Sheridan, R. L., and R. G. Tompkins, "Skin substitutes in burns," *Burns*, Vol. 25, no. 2, pp. 97–103, 1999.

32. Siritientong, T., A. Angspatt, J. Ratanavaraporn, and P. Aramwit, "Clinical potential of a silk sericin-releasing bioactive wound dressing for the treatment of split-thickness skin graft donor sites," 2014.

33. Naimer, S. A., and F. Chemla, "Elastic adhesive dressing treatment of bleeding wounds in trauma victims," *The American journal of emergency medicine*, Vol. 18, no. 7, pp. 816–819, 2000.

34. Winter, G., "Formation of the scab and the rate of epithelisation of superficial wounds in the skin of the young domestic pig," 1962.

35. Barnett, S., and S. Irving, "Studies of wound healing and the effect of dressings," *High performance biomaterials. Lancaster: Technonic*, pp. 583–620, 1991.

36. Agrawal, P., S. Soni, G. Mittal, and A. Bhatnagar, "Role of Polymeric Biomaterials as Wound Healing Agents," *The International Journal of Lower Extremity Wounds*, Vol. 13, no. 3, pp. 180–190, 2014.

37. Williams, D., "Advanced Applications for Materials Implanted within the Human Body," 1987.

38. Nagel, B., H. Dellweg, and L. Gierasch, "Glossary for chemists of terms used in biotechnology (iupac recommendations 1992)," *Pure and Applied Chemistry*, Vol. 64, no. 1, pp. 143–168, 1992.

39. Kim, B., C. Baez, and A. Atala, "Biomaterials for tissue engineering.," *World journal of urology*, Vol. 18, no. 1, pp. 2–9, 2007.

40. Aramwit, P., *Introduction to biomaterials for wound healing*, Vol. 2, Elsevier Ltd, 2016.

41. Mogosanu, G. D., and A. M. Grumezescu, "Natural and synthetic polymers for wounds and burns dressing," *International Journal of Pharmaceutics*, Vol. 463, no. 2, pp. 127–136, 2014.

42. Garg, T., O. Singh, S. Arora, and R. Murthy, "Scaffold: a novel carrier for cell and drug delivery," *Critical Reviews in Therapeutic Drug Carrier Systems*, Vol. 29, no. 1, 2012.

43. Wright, K. A., K. B. Nadire, P. Busto, R. Tubo, J. M. McPherson, and B. M. Wentworth, "Alternative delivery of keratinocytes using a polyurethane membrane and the implications for its use in the treatment of full-thickness burn injury," *Burns*, Vol. 24, no. 1, pp. 7–17, 1998.

44. Pachulski, R., M. Zasadil, D. Adkins, and B. Hanif, "High incidence of pellethane 90a lead malfunction," *Europace*, Vol. 4, no. 1, pp. 45–47, 2002.

45. Van den Kerckhove, E., K. Stappaerts, W. Boeckx, B. Van den Hof, S. Monstrey, A. Van der Kelen, and J. De Cubber, "Silicones in the rehabilitation of burns: a review and overview," *Burns*, Vol. 27, no. 3, pp. 205–214, 2001.

46. Park, S.-N., H. J. Lee, K. H. Lee, and H. Suh, "Biological characterization of edc-crosslinked collagen–hyaluronic acid matrix in dermal tissue restoration," *Biomaterials*, Vol. 24, no. 9, pp. 1631–1641, 2003.

47. Lee, C. H., A. Singla, and Y. Lee, "Biomedical applications of collagen," *International journal of pharmaceutics*, Vol. 221, no. 1, pp. 1–22, 2001.

48. Wade, L., ed., *Wound Healing: Cellular Mechanisms, Alternative Therapies and Clinical Outcomes*, Nova Biomedical, 2015.

49. Rao, S. B., and C. P. Sharma, "Use of chitosan as a biomaterial: Studies on its safety and hemostatic potential," *Journal of Biomedical Materials Research*, Vol. 34, no. 1, pp. 21–28, 1997.

50. Lee, K. Y., and D. J. Mooney, "Alginate: Properties and biomedical applications," *Progress in Polymer Science (Oxford)*, Vol. 37, no. 1, pp. 106–126, 2012.

51. Sun, J., and H. Tan, "Alginate-based biomaterials for regenerative medicine applications," *Materials*, Vol. 6, no. 4, pp. 1285–1309, 2013.

52. Andersen, T., B. L. Strand, K. Formo, E. Alsberg, and B. E. Christensen, "Alginates as Biomaterials in Tissue Engineering," *Carbohydr. Chem*, Vol. 37, pp. 227–258, 2012.

53. Martinsen, A., G. Skjåk-Bræk, and O. Smidsrød, "Alginate as immobilization material: I. correlation between chemical and physical properties of alginate gel beads," *Biotechnology and bioengineering*, Vol. 33, no. 1, pp. 79–89, 1989.

54. Tønnesen, H. H., and J. Karlsen, "Alginate in drug delivery systems," *Drug development and industrial pharmacy*, Vol. 28, no. 6, pp. 621–630, 2002.

55. Draget, K., G. Skjåk-Bræk, B. Christensen, O. Gåserød, and O. Smidsrød, "Swelling and partial solubilization of alginic acid gel beads in acidic buffer," *Carbohydrate Polymers*, Vol. 29, no. 3, pp. 209–215, 1996.

56. Rinaudo, M., "Main properties and current applications of some polysaccharides as biomaterials," 2008.

57. Rani, P., S. Mishra, and G. Sen, "Microwave based synthesis of polymethyl methacrylate grafted sodium alginate: its application as flocculant," *Carbohydrate polymers*, Vol. 91, no. 2, pp. 686–692, 2013.

58. Li, Z., H. R. Ramay, K. D. Hauch, D. Xiao, and M. Zhang, "Chitosan–alginate hybrid scaffolds for bone tissue engineering," *Biomaterials*, Vol. 26, no. 18, pp. 3919–3928, 2005.

59. Beyer, M., J. Reichert, E. Heurich, K. D. Jandt, and B. W. Sigusch, "Pectin, alginate and gum arabic polymers reduce citric acid erosion effects on human enamel," *dental materials*, Vol. 26, no. 9, pp. 831–839, 2010.

60. Ionita, M., M. A. Pandele, and H. Iovu, "Sodium alginate/graphene oxide composite films with enhanced thermal and mechanical properties," *Carbohydrate Polymers*, Vol. 94, no. 1, pp. 339–344, 2013.

61. Kawaguchi, M., T. Fukushima, T. Hayakawa, N. Nakashima, Y. Inoue, S. Takeda, K. Okamura, and K. Taniguchi, "Preparation of carbon nanotube-alginate nanocomposite gel for tissue engineering," *Dental materials journal*, Vol. 25, no. 4, pp. 719–725, 2006.

62. Zhang, Y., Y. Xu, Z. Li, T. Chen, S. M. Lantz, P. C. Howard, M. G. Paule, W. Slikker, F. Watanabe, T. Mustafa, A. S. Biris, and S. F. Ali, "Mechanistic toxicity evaluation of uncoated and PEGylated single-walled carbon nanotubes in neuronal PC12 cells," *ACS Nano*, Vol. 5, no. 9, pp. 7020–7033, 2011.

63. Yang, W., P. Thordarson, J. J. Gooding, S. P. Ringer, and F. Braet, "Carbon nanotubes for biological and biomedical applications," *Nanotechnology*, Vol. 18, no. 41, p. 412001, 2007.

64. Chen, D., H. Feng, and J. Li, "Graphene Oxide : Preparation , Functionalization , and Electrochemical Applications," *Chemical Reviews*, Vol. 10.1021, 2012.

65. Thomas, S., *Surgical dressings and wound management*, Dr Stephen Thomas, 2010.

66. Cowan, T., *Wound care handbook: 2001-2012: the comprehensive guide to product selection*, MA Healthcare, 2011.

67. Chrisman, C. A., "Care of chronic wounds in palliative care and end-of-life patients," 2010.

68. Thomas, S., "Alginate dressings in surgery and wound management–Part 1.," 2000.

69. Kuilla, T., S. Bhadra, D. H. Yao, N. H. Kim, S. Bose, and J. H. Lee, "Recent advances in graphene based polymer composites," *Progress in Polymer Science*, Vol. 35, no. 11, pp. 1350–1375, 2010.

70. McNaught, A. D., A. Wilkinson, *et al.*, "Compendium of chemical terminology. iupac recommendations," 1997.

71. Yang, Y., A. M. Asiri, Z. Tang, D. Du, and Y. Lin, "Graphene based materials for biomedical applications," *Materials Today*, Vol. 16, no. 10, pp. 365–373, 2013.

72. Zhu, Y., S. Murali, W. Cai, X. Li, J. W. Suk, J. R. Potts, and R. S. Ruoff, "Graphene and graphene oxide: synthesis, properties, and applications," *Advanced materials*, Vol. 22, no. 35, pp. 3906–3924, 2010.

73. Goenka, S., V. Sant, and S. Sant, "Graphene-based nanomaterials for drug delivery and tissue engineering," *Journal of Controlled Release*, Vol. 173, pp. 75–88, 2014.

74. Li, J.-L., K. N. Kudin, M. J. McAllister, R. K. Prud'homme, I. A. Aksay, and R. Car, "Oxygen-driven unzipping of graphitic materials," *Physical review letters*, Vol. 96, no. 17, p. 176101, 2006.

75. Meyer, J. C., A. K. Geim, M. I. Katsnelson, K. S. Novoselov, T. J. Booth, and S. Roth, "The structure of suspended graphene sheets," *Nature*, Vol. 446, no. 7131, pp. 60–63, 2007.

76. Nasrollahzadeh, M., F. Babaei, P. Fakhri, and B. Jaleh, "Synthesis, characterization, structural, optical properties and catalytic activity of reduced graphene oxide/copper nanocomposites," *RSC Advances*, Vol. 5, no. 14, pp. 10782–10789, 2015.

77. He, Y., N. Zhang, Q. Gong, H. Qiu, W. Wang, Y. Liu, and J. Gao, "Alginate/graphene oxide fibers with enhanced mechanical strength prepared by wet spinning," *Carbohydrate Polymers*, Vol. 88, no. 3, pp. 1100–1108, 2012.

78. Dreyer, D. R., S. Park, C. W. Bielawski, and R. S. Ruoff, "The chemistry of graphene oxide," *Chemical Society Reviews*, Vol. 39, no. 1, pp. 228–240, 2010.

79. Reshma, S., and P. Mohanan, "Graphene: A multifaceted nanomaterial for cutting edge biomedical application," *Int J Med Nano Res*, Vol. 1, no. 003, 2014.

80. Tang, M., Q. Song, N. Li, Z. Jiang, R. Huang, and G. Cheng, "Enhancement of electrical signaling in neural networks on graphene films," *Biomaterials*, Vol. 34, no. 27, pp. 6402–6411, 2013.

81. Liu, S., T. H. Zeng, M. Hofmann, E. Burcombe, J. Wei, R. Jiang, J. Kong, and Y. Chen, "Antibacterial activity of graphite, graphite oxide, graphene oxide, and reduced graphene oxide: membrane and oxidative stress," *Acs Nano*, Vol. 5, no. 9, pp. 6971–6980, 2011.

82. Depan, D., B. Girase, J. Shah, and R. Misra, "Structure–process–property relationship of the polar graphene oxide-mediated cellular response and stimulated growth of osteoblasts on hybrid chitosan network structure nanocomposite scaffolds," *Acta biomaterialia*, Vol. 7, no. 9, pp. 3432–3445, 2011.

83. Qi, Y., Z. Tai, D. Sun, J. Chen, H. Ma, X. Yan, B. Liu, and Q. Xue, "Fabrication and characterization of poly (vinyl alcohol)/graphene oxide nanofibrous biocomposite scaffolds," *Journal of Applied Polymer Science*, Vol. 127, no. 3, pp. 1885–1894, 2013.

84. Wang, J., C. Liu, Y. Shuai, X. Cui, and L. Nie, "Controlled release of anticancer drug using graphene oxide as a drug-binding effector in konjac glucomannan/sodium alginate hydrogels," *Colloids and Surfaces B: Biointerfaces*, Vol. 113, pp. 223–229, 2014.

85. Li, J., Y. Wu, J. He, and Y. Huang, "A new insight to the effect of calcium concentration on gelation process and physical properties of alginate films," *Journal of Materials Science*, Vol. 51, no. 12, pp. 5791–5801, 2016.

86. Kirdponpattara, S., A. Khamkeaw, N. Sanchavanakit, P. Pavasant, and M. Phisalaphong, "Structural modification and characterization of bacterial cellulose–alginate composite scaffolds for tissue engineering," *Carbohydrate polymers*, Vol. 132, pp. 146–155, 2015.

87. Gupta, N. V., and H. Shivakumar, "Investigation of swelling behavior and mechanical properties of a ph-sensitive superporous hydrogel composite," *Iranian journal of pharmaceutical research: IJPR*, Vol. 11, no. 2, p. 481, 2012.

88. Stoppel, W. L., J. C. White, S. D. Horava, A. C. Henry, S. C. Roberts, and S. R. Bhatia, "Terminal sterilization of alginate hydrogels: efficacy and impact on mechanical properties," *Journal of Biomedical Materials Research Part B: Applied Biomaterials*, Vol. 102, no. 4, pp. 877–884, 2014.

89. Luo, B., B. Wang, M. Liang, J. Ning, X. Li, and L. Zhi, "Reduced graphene oxide-mediated growth of uniform tin-core/carbon-sheath coaxial nanocables with enhanced lithium ion storage properties," *Advanced Materials*, Vol. 24, no. 11, pp. 1405–1409, 2012.

90. Tripathi, P., C. Patel, R. Prakash, M. Shaz, and O. Srivastava, "Synthesis of high-quality graphene through electrochemical exfoliation of graphite in alkaline electrolyte," *arXiv preprint arXiv:1310.7371*, 2013.

91. Banazadeh, A., S. Mozaffari, and B. Osoli, "Facile synthesis of cysteine functionalized magnetic graphene oxide nanosheets: Application in solid phase extraction of cadmium from environmental sample," *Journal of Environmental Chemical Engineering*, Vol. 3, no. 4, pp. 2801–2808, 2015.

92. Nikolić, V. D., D. P. Ilić, L. B. Nikolić, M. Z. Stanković, L. P. Stanojević, I. M. Savić, and I. M. Savić, "The synthesis and structure characterization of deoxyalliin and alliin," *Advan Technol*, Vol. 1, pp. 38–46, 2012.

93. Peretz, S., M. Florea, D.-F. Anghel, D. Bala, C. Stoian, and G. Zghera, "Preparation of porous calcium alginate beads and their use for adsorption of o-nitrophenol from aqueous solutions,"

94. Bouhadir, K. H., K. Y. Lee, E. Alsberg, K. L. Damm, K. W. Anderson, and D. J. Mooney, "Degradation of partially oxidized alginate and its potential application for tissue engineering," *Biotechnology progress*, Vol. 17, no. 5, pp. 945–950, 2001.

95. Daemi, H., and M. Barikani, "Synthesis and characterization of calcium alginate nanoparticles, sodium homopolymannuronate salt and its calcium nanoparticles," *Scientia Iranica*, Vol. 19, no. 6, pp. 2023–2028, 2012.

96. Lee, K. Y., J. A. Rowley, P. Eiselt, E. M. Moy, K. H. Bouhadir, and D. J. Mooney, "Controlling mechanical and swelling properties of alginate hydrogels independently by cross-linker type and cross-linking density," *Macromolecules*, Vol. 33, no. 11, pp. 4291–4294, 2000.

97. Dong, J., Z. Yao, T. Yang, L. Jiang, and C. Shen, "Control of superhydrophilic and superhydrophobic graphene interface," *Scientific reports*, Vol. 3, 2013.

98. Qian, L., and H. Zhang, "Controlled freezing and freeze drying: a versatile route for porous and micro-/nano-structured materials," *Journal of chemical technology and biotechnology*, Vol. 86, no. 2, pp. 172–184, 2011.

99. Ciriza, J., L. S. del Burgo, M. Virumbrales-Muñoz, I. Ochoa, L. Fernandez, G. Orive, R. Hernandez, and J. Pedraz, "Graphene oxide increases the viability of c 2 c 12 myoblasts microencapsulated in alginate," *International journal of pharmaceutics*, Vol. 493, no. 1, pp. 260–270, 2015.

100. Spitzer, R.-S., C. Perka, K. Lindenhayn, and H. Zippel, "Matrix engineering for osteogenic differentiation of rabbit periosteal cells using α-tricalcium phosphate particles in a three-dimensional fibrin culture," *Journal of biomedical materials research*, Vol. 59, no. 4, pp. 690–696, 2002.

101. Çelik, E., C. Bayram, R. Akçapınar, M. Türk, and E. B. Denkbaş, "The effect of calcium chloride concentration on alginate/fmoc-diphenylalanine hydrogel networks," *Materials Science and Engineering: C*, Vol. 66, pp. 221–229, 2016.